Journal of Vibration Engineering & Technologies (2023) 11:845–872
https://doi.org/10.1007/s42417-022-00612-x

ORIGINAL PAPER

Sensitivity Analysis of Random Frequency Responses of Hybrid Multi-functionally Graded Sandwich Shells

Vaishali[1] · S. Kushari[1] · R. R. Kumar[2] · P. K. Karsh[3] · S. Dey[1]

Received: 11 April 2022 / Revised: 17 June 2022 / Accepted: 22 June 2022 / Published online: 19 July 2022

Abstract

Purpose This paper presents the sensitivity analysis (SA) of the random natural frequency responses of hybrid multi-functionally graded sandwich (HMGS) shells for establishing a unified measure in the case of multi-objective performances. The functionally graded materials, laminated composites, and sandwich cores are employed to develop such novel structures to tailor the benefits of each component in a single structure.

Methods A novel MARS-based sensitivity analysis of these hybrid multi-functionally graded sandwich shells is developed to achieve computational efficiency without compromising with the outcome. Such surrogate-assisted FE approaches are crucial for computationally intensive multi-objective systems. The basic governing equations of random natural frequency are framed based on finite element formulation. The variabilities of major influencing random input parameters (here, geometric and material properties) are carried out by employing Monte Carlo simulation (MCS). The multivariate adaptive regression spline (MARS) is adopted as a surrogate model to increase computational efficiency.

Results and Conclusion The results are portrayed to showcase the significant effects of variable input parameters (sensitivity) on random frequency responses of such novel HMGS shells. Hence, it provides the predominant random input parameters and their relative degree of importance while designing such multi-dimensional structural systems. Thus, the contribution of this article lies in both the development of a computationally efficient sensitivity analysis approach and the insightful numerical results for hybrid structures presented thereafter. The comprehensive and collective sensitivity quantification considering multi-functional objectives, as presented in this article, would lead to efficient computational modelling of complex structural systems for more optimized designs and better quality control during manufacturing.

Keywords Sensitivity analysis (SA) · Hybrid multi-functionally graded sandwich (HMGS) shells · Multivariate adaptive regression spline (MARS) · Monte Carlo simulation (MCS)

Introduction

Sandwich structures are exhaustively employed in spacecraft, civil structures, high-speed transportations, and automotive industries [1, 2] due to their tailored multi-functional features. In general, the sandwich structure construction comprises three parts: upper facesheet, lower facesheet, and middle core. The facesheets consist of a laminated composite structure having excessive stiffness and strength, and the core is made of foam [3] structure with low density to impart low weight. These structures have high energy absorption and impact resistance [4–6]. The functionally graded materials (FGM) are composed of two main constitutes, namely ceramic and metal. In FGM, one free surface is metal-rich, providing high strength and stiffness to the structure. In contrast, the other free surface is ceramic-rich, providing sustainability to its strength at elevated temperature and resistance to corrosion. Due to limitations in sandwich structures such as low temperature-resistant and corrosion-resistant properties, its facesheet can be replaced by functionally graded materials (FGM) instead of laminated composites. Therefore, combining both sandwich and

✉ S. Kushari
subrata734@gmail.com

[1] Department of Mechanical Engineering, National Institute of Technology Silchar, Silchar, India

[2] Department of Aeronautical Engineering, Hindustan Institute of Technology and Science, Chennai, India

[3] Department of Mechanical Engineering, Parul Institute of Engineering and Technology, Parul University, Vadodara, India

functionally graded structures, the hybrid multi-functionally graded sandwich (HMGS) shell is idealised in the present study, exhibiting the novelty of superiority and tailoring in properties.

In the past, studies related to such structures were conducted by Tung [7] for the post-buckling, bending, and buckling behaviour of these FG-sandwich plates. The finite element method (FEM) is incorporated to design FG-sandwich plates by employing shear deformation theories [8]. Later on, some researchers [9–14] developed various computational models for dynamic characteristics of hybrid functionally graded (FG)-sandwich structure. On referring to these works of literature, generalised observations are obtained. First, advanced computational methods are primarily required for analysing these hybrid FG-sandwich structures. Second, these hybrid structures are employed in advanced applications, and third, it performs better than the conventional sandwich structures. Therefore, the present study focuses on a computational framework for mapping triggering parameter sensitivity (both geometric and material properties). Hence, a novel functional class of HMGS shells is considered for random free vibration. In the present study, six cases are categorised to analyse these hybrid structures as described in Table 1 and furnished in Fig. 1.

In aerospace, civil construction, naval, and automobile sectors, hybrid FG shell-type structures play a vital role. But while using shell-type forms, it is challenging to maintain the standard, as they often lead to non-conformity from their deterministic design specification. In addition, the manufacturing processes of these HMGS structures are pretty complicated due to multiple sources of uncertainties. The overall responses have notable stochastic variations because of these uncontrollable fluctuations (material properties and geometric variation). Therefore, adopting such methods is essential to design safe and reliable hybrid structures. Therefore, it is critically needed to consider these uncertainties by promoting an exclusive method for analysing such structures. Hence, the present study is aimed to investigate the sensitivity of elliptical paraboloid, cylindrical, hyperbolic paraboloid, and spherical-shaped HMGS shells (Fig. 2) towards their stochastic dynamic responses.

Many researchers worked on a deterministic approach for dynamic analyses of plate and shell structures [15–18].

Table 1 Shell geometries created on considering $a=2$ in the present study (a = numerical value of R_x and R_y, *and* R_x and R_y is the radius of curvature in x and y direction, respectively)

Radius of curvature	Geometry				
	S_{plate}	S_{cyl}	S_{sph}	S_{ell}	S_{hyp}
R_x	Infinite	a	a	a	a
R_y	Infinite	Infinite	a	$2a$	$-a$

An analytical study is performed for the dynamic response of sandwich structures under blast loading [19]. Cui et al. [20] and Zhu et al. [21] worked on sandwich plates having square geometry to find the analytical solution for the dynamic response using the energy balance method. Under blast loading, dynamic responses are studied on rectangular sandwich plates [22, 23]. Dharmasena et al. [24] worked on metal honeycomb sandwich structures under the influence of explosive loading. They observed that the small impulse causes the bending of the plate near the load, and the core gradually buckle. Cui et al. [25] and Zhu et al. [26] worked on a honeycomb sandwich structure with a tetrahedral lattice structured core. The obtained results illustrate that tetrahedral design portrays better impact resistance than the hexagonal sandwich core. Jamil et al. [27] worked on Al-thermoplastic polyurethane sandwich structures and found that the structure executed better blast resistance by adding thermoplastic polyurethane. Reyes [28] applied the energy balance approach to study the impact behaviour of the sandwich structure having thermoplastic fiber–metal laminated facesheet and Al-based core. The result indicates that the residual flexural strength is increased significantly. Low-velocity impact behaviour of sandwich structure having Al-core and glass fiber reinforced polypropylene-fiber–metal laminated facesheet is investigated [29]. Liu et al. [30, 31] worked on an Al-based core and fibre-metal laminated facesheet, wherein low-velocity impact response is studied and then switched to high-velocity impact response. Basturk et al. [32] studied the dynamic response of fiber–metal laminated Al-based core sandwich plate. Six porous models were considered to analyse the wave propagation of a ceramic–metal functionally graded sandwich plate. It was found that fluctuation in hygro-thermal stresses and moisture content plays an important role [33]. Similarly, three different orientations of sandwich beams were considered to analyse the natural frequencies of an FG material. The layup schemes and thickness ratio of skin–core-skin have vital importance in evaluating the non-dimensional natural frequencies [34]. An optimised shear deformation theory was developed for sandwich structures with FG facesheet and FG hardcore [35]. A square sandwich plate was considered to analyse the free vibration of a porous FG material. A varied boundary condition was presented to investigate the effects of porosity in volume fraction, lay-up configuration, and thickness ratio [36]. On the same note, a variation in moisture and temperature was conducted to analyse the free vibration of the FG-sandwich plate. The results show that the damping coefficient is directly proportional to the free vibration of the material [37]. A reliable design was proposed to analyse the thermo-mechanical properties of FG steel incorporating Fourier series expansion and the Galerkin method [38]. Similarly, free vibrational analyses of FG conical shell panels suggested that thickness and boundary

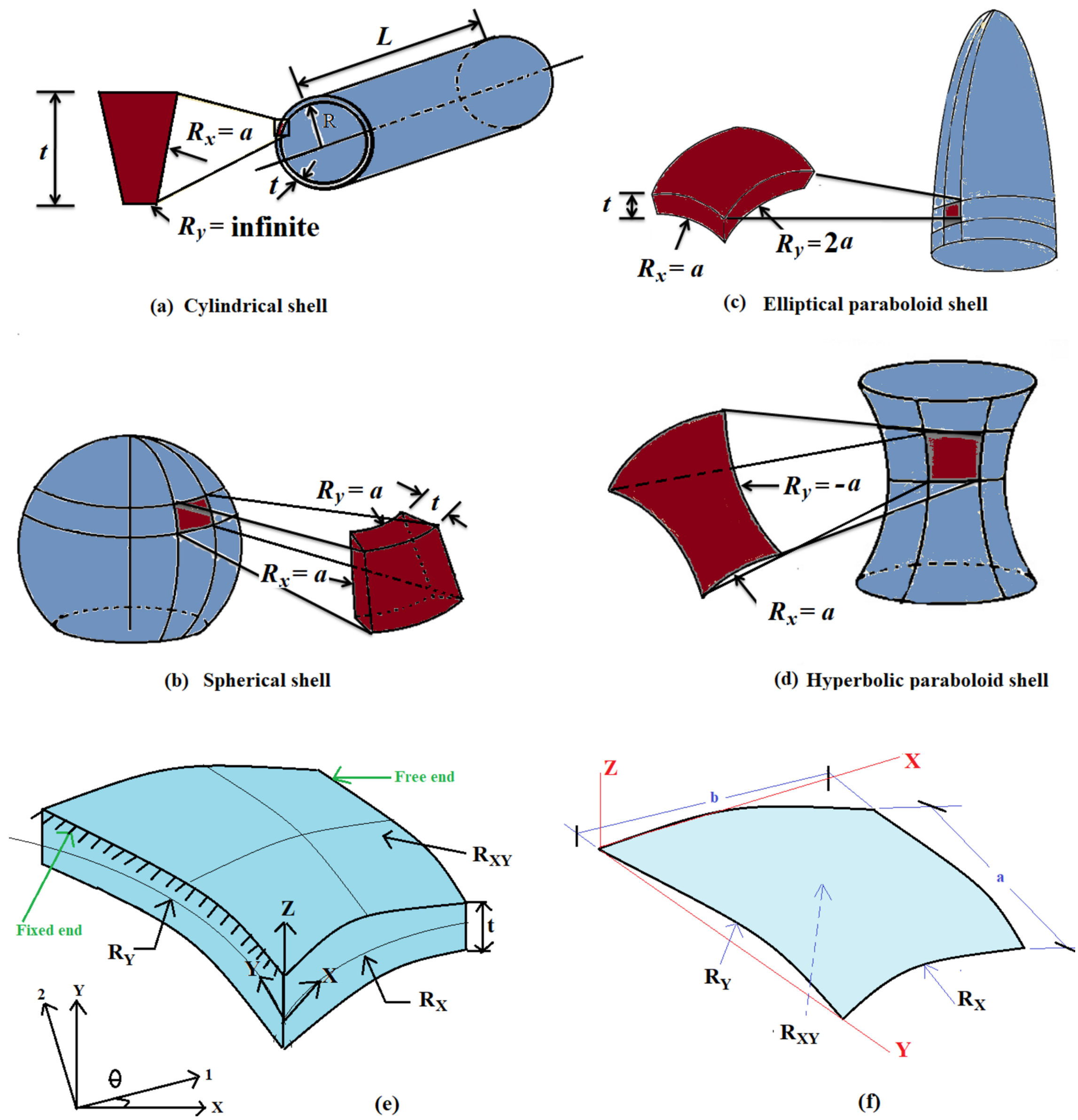

Fig. 1 Geometric configurations of HMGS shells: **a** cylindrical ($S_{cyl.}$), **b** spherical ($S_{sph.}$), **c** elliptical paraboloid ($S_{ell.}$), and **d** hyperbolic paraboloid ($S_{hyp.}$) and **e**, **f** shell model

conditions have significant effects. A mesh-free Ritz method was employed to perform the analysis [39]. An analytical approach based on Fourier series and Laplace transformation is incorporated to analyse FG piezoelectric cylindrical panels [40]. The hygro-thermal and mechanical behaviour was analysed for FG ceramic plate to investigate the effects of moisture, temperature, and damping coefficients [41]. A bending analysis was performed utilising higher-order shear deformation theory, and a Navier-type solution was obtained under transverse loading conditions [42]. Buckling and free vibration analyses were carried out for functionally graded carbon nanotube-reinforced quadrilateral and skew laminates [45]. Detailed numerical results were obtained by the discrete singular convolution method. An alteration in the weight fraction of carbon nanotubes was considered to analyse the static stability analysis of carbon nanotube reinforced polymeric composite [48]. An imperfect porous FG plate was considered to analyse the free vibrational response, considering the cut-out effect, geometric variation, and volume fraction [49]. More work on functionally graded structures is presented in various literature [37, 43–47, 50–53]. The literature mentioned above summarised that extensive work on sandwich and FGM structure is carried out. But, the studies on the dynamic response of hybrid structures are limited. In a real-life situation, the sources of uncertainty should be considered for the reliability and safety

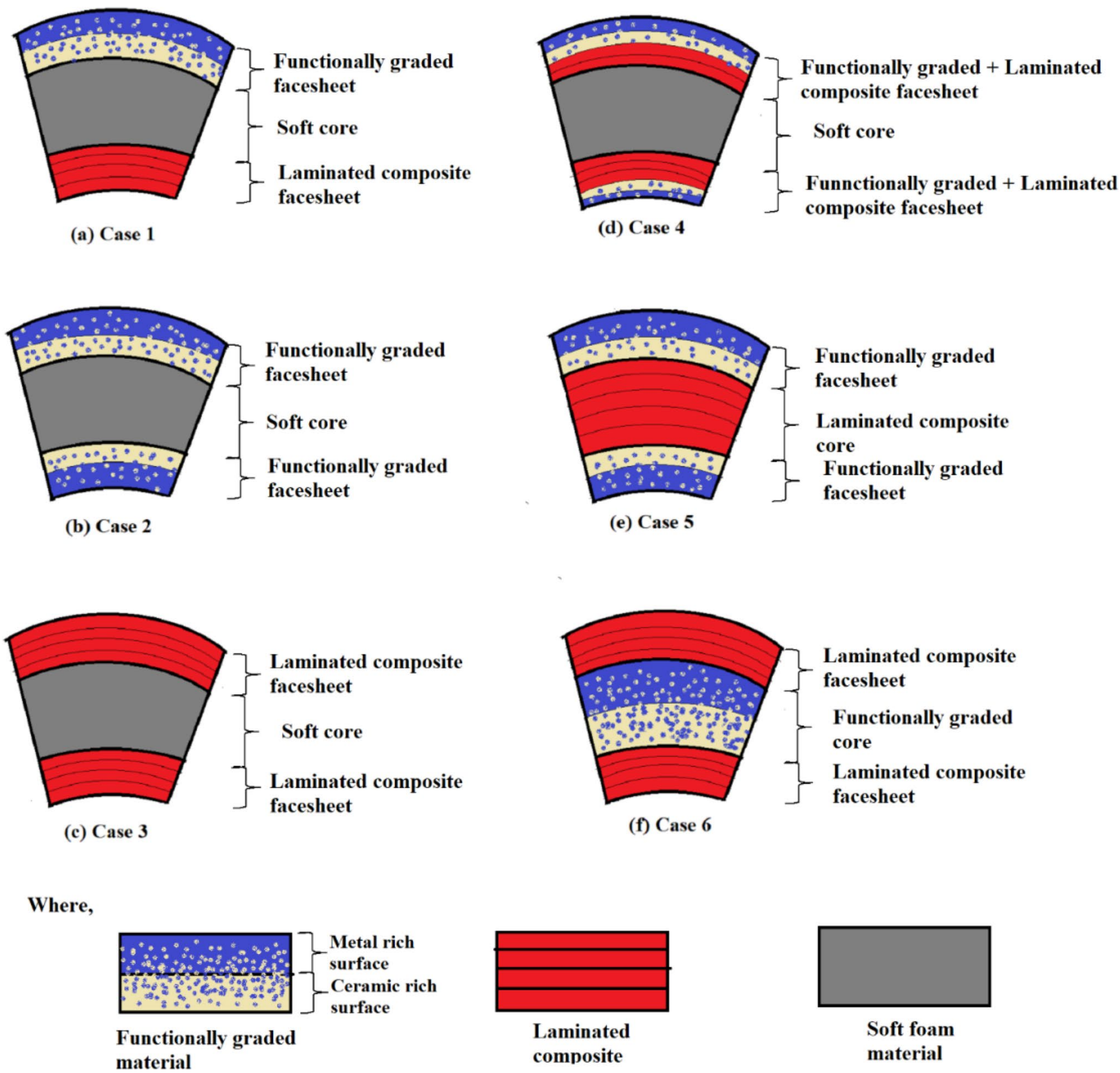

Fig. 2 Six cases of hybrid multi-functionally graded sandwich (HMGS) structures

of these structures. Monte Carlo simulation (MCS) is one of the most preferred approaches for probabilistic modelling. This technique's effectiveness lies in how the random numbers are generated from the pseudo-random number generator. The limitation of this technique is high computational cost and time. MCS is quite an expensive process; the quality of uncertainty prediction directly depends on the number of simulations. Therefore, surrogate models are integrated with the MCS technique to overcome this problem and the computationally efficient overall process. Some literature [54–61] showcased utilising MCS and MARS in the stochastic domain to analyse the natural frequency of FGM cantilever plates at different temperatures. For the present study, MARS is integrated with the finite element framework.

In the past, the sensitivity analysis is linked with the material properties and geometric shape and size [62–73]. Many researchers focussed on sensitivity analysis while considering buckling, statics, and transient response problems. In the deterministic regime, sensitivity analysis involved two methods, namely, variational and implicit differentiation [74, 75]. The variational method requires differentiation of the structural response continuum governing equations. Still, this method cannot be applied under challenging problems, while the implicit differentiation method involves the derivation of the discrete formulations of the FE method. Therefore, the latter method became more popular. Later on, the sensitivity analysis is further classified into two parts, namely, local sensitivity and global sensitivity, respectively. The local sensitivity is computed based on the derivate of the response function, while the global sensitivity considers the overall response behaviour. Therefore, it is evident that local sensitivity is more accessible to compute than global sensitivity. The only disadvantage is that it considers sensitivity concerning the base point, which is less critical. The global sensitivity analysis is preferred for determining the overall response behaviour; it deals with system stochasticity. But there are some limitations to these global sensitivity analyses as they require extensive function evaluations; therefore, it becomes computationally expensive and requires enormous time and cost. Surrogate-based global sensitivity is adapted to overcome these limitations. This method aims to make the process computationally efficient by reducing expensive simulations. Hamdia et al. [76].

Hamdia et al. [76] worked on flexo-electric material for sensitivity analysis. Three surrogate models are employed: extended Fourier amplitude, PCE-Sobol, and Morris One-At-a-Time model. Antonio and Hoffbauer [77] performed reliability and sensitivity analysis of composite structures, determining random input parameter's effect by utilising ANN integrated with MCS. Zhang et al. [78] worked on composite beam damage detection and performed a sensitivity analysis to analyse noise's effect. Sensitivity analysis is adapted on laminated composites utilising the topological derivative mapping method to obtain optimal design [79]. Bishay and Sofi [80] performed sensitivity analysis on composites to construct robotic fingers. A comparative study of variance moment independent based method is conducted by Zadeh et al. [81], whereas Zhao and Bu [82] worked on global sensitivity analysis considering hierarchical sparse meta-modelling approach. Vu-Bac et al. [83] developed software to analyse the probabilistic sensitivity for computationally expensive models.

The earlier discussion concludes that most studies related to the dynamic analysis of hybrid structures are carried out in a deterministic framework. In real-life situations, various uncertainties are involved in every system, which is unavoidable. These uncertainties can be material properties and geometric uncertainties, environmental uncertainties. Therefore, for the safety and reliability of the system, these uncertainties should not be neglected. The stochastic dynamic analysis in the case of hybrid FG-sandwich structure is scarce in past literature. The manufacturing of these hybrid structures is quite complex; in addition to it, the shell-type construction adds to its complexity. Therefore, there is a great chance that the designed structure will contain deviation from the initial design specification. The stochastic study plays great importance as it considers these uncertainties while carrying out the analysis, making the study more reliable. The present study includes the sensitivity analysis in conjunction with random frequency responses of HMGS shells considering various shell geometries and various cases (based on the construction of a hybrid structure). The sensitivity analysis of such structures for dynamic analysis considering traditional MCS is computationally expensive. The MARS model is constructed and integrated with the finite element framework to avoid it. With this analysis, the relative effects of individual material and geometric properties are portrayed in the light of the structure's uncertain global frequency response. There lie two novelties in the present work. This is the first attempt to incorporate MARS with the efficient MCS for stochastic dynamic analysis of HMGS shells. As discussed earlier that MCS is quite an exhaustive process, requiring excessive time and cost. Therefore, implementing the surrogate (here, MARS) with the FE model makes the process computationally efficient. This surrogate-based approach enhances efficiency when dealing with a complex and realistic system. To the best of the authors' knowledge, this is the first attempt to perform the sensitivity analysis of HMGS shells with different geometries and structural forms. From the earlier discussion, it is known that manufacturing these HMGS structures is pretty complicated, involving multiple sources of uncertainty. Because of these uncontrollable fluctuations (material properties and geometric variation), there is a notable amount of stochastic variation in the system's overall response. Therefore, adopting such methods is essential to design a safe and reliable structure. Therefore, it is critical to consider these uncertainties and have an exclusive method for analysing such structures. Such detailed, exhaustive studies are needed while designing such structures.

Theoretical Formulation

The present study deals with hybrid multi-functionally graded sandwich (HMGS) shells with cantilever boundary conditions. The different shell geometries are considered, such as spherical, hyperbolic paraboloid, cylindrical, and elliptical paraboloid geometries (Fig. 1 and Table 1). Six different cases of HMGS (Fig. 2 and Table 2) are considered for the sensitivity analysis in conjunction with random frequency responses.

Governing Equation

To obtain the material properties FGM sheet, power-law [84, 85] is employed, and the same is expressed as,

Table 2 Six cases of hybrid multi-functionally graded sandwich (HMGS) structures

Cases	Facesheet	Core
Case 1	Upper facesheet-laminated composite and lower facesheet-FGM	Softcore
Case 2	FGM	Softcore
Case 3	Laminated composite	Softcore
Case 4	FGM and laminated composite	Softcore
Case 5	FGM	Laminated composite
Case 6	Laminated composite	FGM

$$\mathbf{A}(h) = \mathbf{A}_{\mathrm{m}} + [\mathbf{A}_{\mathrm{c}} - \mathbf{A}_{\mathrm{m}}]\left[\frac{(2z+h)}{2h}\right]^{n}, \tag{1}$$

where n represents the power-law index, A represents the various material properties. Here, A_{m} indicate the properties of metal while A_{c} shows the properties of ceramics. In the above equation, h represents the thickness/depth of the FGM plate, whereas $z = {}^{-t}/_{2}$ and $z = {}^{t}/_{2}$ indicates the upper and lower layer of the plate, and x represents the power-law exponent. Here, the temperature-dependent material properties are expressed as [86],

$$A = A_0 + A_{-1}T^{-1} + 1 + A_1 T + A_2 T^2 + A_3 T^3, \tag{2}$$

where T represents the temperature value in Kelvin and A_0 ,A_{-1},A_1,A_2 and A_3 are the values of temperature coefficients. According to the first-order shear deformation theory, the following Eqs. (3), (4), and (5) are employed to represent the displacement field as,

$$a(x,y,z)(\varpi) = a_0(x,y)(\varpi) - za(x,y)(\varpi)\mathcal{R}_x(x,y)(\varpi), \tag{3}$$

$$b(x,y,z)(\varpi) = b_0(x,y)(\varpi) - zb(x,y)(\varpi)\mathcal{R}_y(x,y)(\varpi), \tag{4}$$

$$c(x,y,z)(\varpi) = c(x,y)(\varpi) = c_0(x,y)(\varpi), \tag{5}$$

where the stochastic displacement in x, y, and z-direction is represented by $a(\varpi)$, $b(\varpi)$ and $c(\varpi)$, respectively, and the stochastic displacement at mid-plane in x, y, and z-direction is represented by $a_0(\varpi)$, $b_0(\varpi)$ and $c_0(\varpi)$ respectively, whereas rotation in the direction of x and y direction is represented by $\mathcal{R}_x(\varpi)$ and $\mathcal{R}_y(\varpi)$ respectively. The symbol '(ϖ)' represents the degree of stochasticity in the respective input parameters. The generalized stochastic dynamic equilibrium equation [9] can be expressed as,

$$\{\ddot{\mathbf{u}}(\varpi)\} + [\mathbf{c}(\varpi)]\{\dot{\mathbf{u}}(\varpi)\} + [\mathbf{k}(\varpi)]\{\mathbf{u}(\varpi)\} = \{f(\varpi)\}, \tag{6}$$

where $\{\mathbf{u}(\varpi)\}$ is the global displacement vector, $[m(\varpi)]$ is the global mass matrix, $[\mathbf{c}(\varpi)]$ is the global damping matrix, $[\mathbf{k}(\varpi)]$ represent the global stiffness matrices, while $\{\mathbf{f}(\varpi)\}$ is an external force vector. Considering free vibration, the above equation can be reduced as,

$$[\mathbf{m}(\varpi)]\{\ddot{\mathbf{u}}(\varpi)\} + [\mathbf{k}(\varpi)]\{\mathbf{u}(\varpi)\} = 0. \tag{7}$$

The static components, as well as time-dependent components, are considered for dynamic analysis. Here, the displacement vector $\{\mathbf{u}(\varpi)\}$ contains both static and a dynamic term $\left[\{\mathbf{u}(\varpi)\} = \left\{\mathbf{u}_s(\varpi)\right\} + \left\{\mathbf{u}_p(\varpi)\right\}\right]$, where $\left\{\mathbf{u}_p(\varpi)\right\}$ is a minor linear time reliant perturbation about $\left\{\mathbf{u}_s(\varpi)\right\}$, while $\left\{\mathbf{u}_s(\varpi)\right\}$ is expressed as the static displaced position. The equation of motion can be stated as,

$$[\mathbf{m}(\varpi)]\left\{\ddot{\mathbf{u}}_{\mathrm{p}}(\varpi)\right\} + [\mathbf{k}(\varpi)]\left(\left\{\mathbf{u}_{\mathrm{p}}(\varpi)\right\} + \left\{\mathbf{u}_{\mathrm{s}}(\varpi)\right\}\right) = 0. \tag{8}$$

Neglecting $\left\{u_{\mathrm{s}}(\varpi)\right\}$, the equation of motion for free vibration can be expressed as,

$$[\mathbf{m}(\varpi)]\left\{\ddot{\mathbf{u}}_{\mathbf{p}}(\varpi)\right\} + [\mathbf{k}(\varpi)]\left\{\mathbf{u}_{\mathbf{p}}(\varpi)\right\} = 0 \tag{9}$$

In Eq. (9), the displacement $\left\{u_{\mathrm{p}}(\varpi)\right\}$ is a function of time and space. In free vibration analysis, the time and space coordinates of displacement function can be expressed as,

$$\left\{\mathbf{u}_{\mathrm{p}}(\varpi)\right\} = \mathbf{A}'\mathrm{e}^{i\omega t}\{\boldsymbol{\theta}\}, \tag{10}$$

$$\left\{\ddot{\mathbf{u}}_{\mathrm{p}}(\varpi)\right\} = -\mathbf{A}'\omega^2\mathrm{e}^{i\omega t}\{\boldsymbol{\theta}\}. \tag{11}$$

On substituting the values of $\left\{\mathbf{u}_{\mathrm{p}}(\varpi)\right\}$ and $\left\{\ddot{\mathbf{u}}_{\mathrm{p}}(\varpi)\right\}$ in Eq. (9), the modified equation is

$$\mathbf{A}'e^{i\omega t}(-\boldsymbol{\omega}^2[\mathbf{m}(\varpi)]\{\boldsymbol{\theta}\} + [\mathbf{k}(\varpi)]\{\boldsymbol{\theta}\}) = 0 \tag{12}$$

As $\mathrm{A}'e^{i\omega t} \neq 0$

$$\boldsymbol{\omega}^2[\mathbf{m}(\varpi)]\{\boldsymbol{\theta}\} = [\mathbf{k}(\varpi)]\{\boldsymbol{\theta}\}. \tag{13}$$

Here, ω imply natural frequencies. Now, utilising the standard eigenvalue problem [62], ω can be evaluated. QR iteration algorithm is employed to solve the equations. Now, Eq. (13) is further transformed as,

$$[\mathbf{A}]\{\boldsymbol{\theta}\} = \boldsymbol{\lambda}(\varpi)\{\boldsymbol{\theta}\} \tag{14}$$

$$[\mathbf{A}] = [\mathbf{k}(\varpi)^{-1}](\mathbf{m}) \text{ and } \boldsymbol{\lambda}(\varpi) = \frac{1}{(\boldsymbol{\omega}(\varpi))^2}. \tag{15}$$

Finite Element Formulation

The finite element formulation of the hybrid shell is designed considering a bending element (eight noded) of an isoperimetric quadratic structure. Each node has (three translational and two rotational) five degrees of freedom. Polynomial shape functions with coordinates ξ, η and ζ

depict the displacement relation between the nodal values and the generalised equation. The interpolation polynomial function is stated as

$$a(\xi,\eta) = F_0 + F_1\xi + F_2\eta + F_3\xi^2 + F_4\xi\eta + F_5\eta^2 + F_6\xi^2\eta + F_7\xi\eta^2, \tag{16}$$

where $F_0, F_1, ...F_7$ are the degrees of freedom.

The shape functions S_i can be shown as:

$$\mathbf{S_i} = 0.25\left(1+\xi\xi_\mathbf{i}\right)\left(\mathbf{1}+\boldsymbol{\eta\eta}_\mathbf{i}\right)\left(\xi\xi_\mathbf{i}+\boldsymbol{\eta\eta}_\mathbf{i}-\mathbf{1}\right) \quad i = 1,\ 2,\ 3,\ 4, \tag{17}$$

$$\mathbf{S}_i = 0.5\left(1+\boldsymbol{\eta\eta}_i\right)\left(1-\xi^\mathbf{2}\right) \quad i = 5, 7$$

$$\mathbf{S}_i = 0.5\left(1+\xi\xi_\mathbf{i}\right)\left(1-\boldsymbol{\eta}^\mathbf{2}\right) \quad i = 6, 8.$$

The shape functions accuracy is given by

$$\sum_{i=1}^{8} \mathbf{S_i} = 1, \ \sum_{i=1}^{8} \frac{\partial \mathbf{S}_i}{\partial \xi} = 0 \text{ and } \sum_{i=1}^{8} \frac{\partial \mathbf{S}_i}{\partial \boldsymbol{\eta}} = 0. \tag{18}$$

The bending formulation by utilising the same shape functions for the coordinates (x,y) is stated as

$$\mathbf{x} = \sum_{i=1}^{8} \mathbf{S_i}\,\mathbf{x_i} \text{ and } \mathbf{y} = \sum_{i=1}^{8} \mathbf{S_i}\,\mathbf{y_i}. \tag{19}$$

The displacement at any point can be shown as (Fig. 3)

$$\begin{aligned}\mathbf{a} &= \sum_{i=1}^{8} \mathbf{S_i}\,\mathbf{a_i},\ \mathbf{b} = \sum_{i=1}^{8} \mathbf{S_i}\,\mathbf{b_i},\ \mathbf{c} = \sum_{i=1}^{8} \mathbf{S_i}\,\mathbf{c_i},\ \boldsymbol{\varphi}_\mathbf{x} \\ &= \sum_{i=1}^{8} \mathbf{S_i}\,\boldsymbol{\varphi}_{xi},\ \boldsymbol{\varphi}_\mathbf{y} = \sum_{i=1}^{8} \mathbf{S_i}\,\boldsymbol{\varphi}_{yi},\end{aligned} \tag{20}$$

$$\text{where, } \begin{bmatrix}\mathbf{N_{i,x}}\\ \mathbf{N_{i,y}}\end{bmatrix} = [\mathbf{J}]^{-1}\begin{bmatrix}\mathbf{N_{i,\xi}}\\ \mathbf{N_{i,\eta}}\end{bmatrix} \text{ and } [\mathbf{J}] = \begin{bmatrix}\mathbf{X_\xi} & \mathbf{Y_\xi}\\ \mathbf{X_\eta} & \mathbf{Y_\eta}\end{bmatrix}. \tag{21}$$

Sensitivity Analysis

Sensitivity analysis (SA) describes the effect of each input parameter and their combined effects on the output responses. The relationship between input and output parameters for a constructed model can be defined as [88]

$$\mathbf{Z} = f(\mathbf{Y_1}, \ldots, \mathbf{Y_n}), \tag{22}$$

where Y_i are the random input variables, by fixing Y_i to be y_i^* one at a time, the conditional variance of the output Var($\mathbf{Z}|\mathbf{Y_i}= \mathbf{y}_i^*$) is generally less than the total variance Var($\mathbf{Z}$), indicating some contribution of variance from the input variable $\boldsymbol{Y_i}$. It states the sensitivity of uncertain output concerning $\boldsymbol{Y_i}$ (input). For all possible values of $\mathbf{y}_i^*$, the variable Var($\mathbf{Z}|\mathbf{Y_i}= \mathbf{y}_i^*$) is a random variable. Thus, we

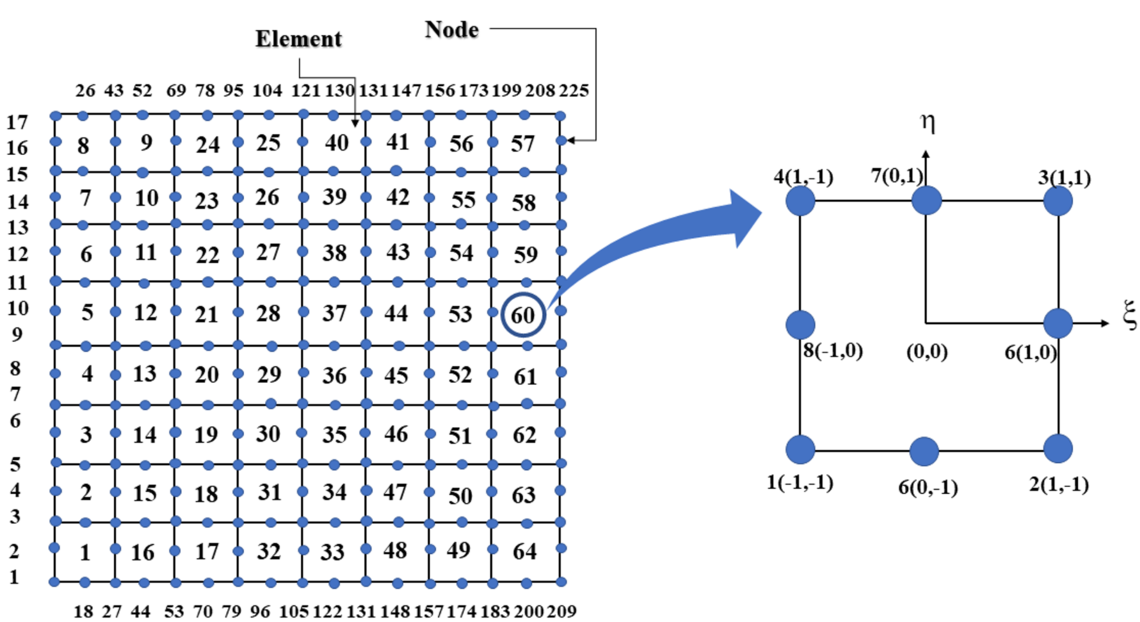

Fig. 3 Discretization model for hybrid sandwich plate (mesh size 8 × 8)

can calculate its expected value E[Var($\mathbf{Z}|\mathbf{Y}_i$)]. To quantify the importance of $\boldsymbol{Y_i}$ (input), one can determine it from a deterministic value Var($\mathbf{Z}$) − E[Var($\mathbf{Z}|\mathbf{Y}_i$)]. Likewise, for all expected values of $\boldsymbol{Y_i}$(input), the conditional expectation is E[Var($\mathbf{Z}|\mathbf{Y_i}$)] which is also a random variable. Therefore, the contribution of Y_i (input) can be depicted by Var($\mathbf{Z}$) − Var(E[$\mathbf{Z}|\mathbf{Y}_i$]) as

$$\mathrm{Var}(\mathbf{Z}) = \mathrm{E}[\mathrm{Var}(\mathbf{Z}|\mathbf{Y}_i)] + \mathrm{Var}(\mathrm{E}[\mathbf{Z}|\mathbf{Y}_i]). \quad (23)$$

To quantify the sensitivity of output related to the uncertainty of the ith input, using Sobol' sensitivity index [67, 68, 89, 90]

$$\mathbf{SI} = \mathrm{Var}(\mathrm{E}[\mathbf{Z}|\mathbf{Y}_i])/\mathrm{Var}(\mathbf{Z}). \quad (24)$$

The higher order sensitivity indices predict the interconnection between input variables. Let $\boldsymbol{Y}_i$ and Y_j are two variables that are taken constantly simultaneously at a time. The combined effect of these two can be measured by Var(E[$\mathbf{Z}|\mathbf{Y_i}, \mathbf{Y}_j$]). The second-order indices are expressed as,

$$\mathbf{SI}_{ij} = \mathrm{Var}(\mathrm{E}[\mathbf{Z}|\mathbf{Y_i}, \mathbf{Y}_j])/\mathrm{Var}(\mathbf{Z}) - \mathbf{SI}_i - \mathbf{SI}_j. \quad (25)$$

Similarly, the equations are derived for higher order indices. Therefore, in general, the total variance can be depicted as

$$\mathrm{Var}(\mathbf{Z}) = \sum\nolimits_i \mathbf{V}_i + \sum\nolimits_{i,j>i} \mathbf{V}_{ij} + \sum\nolimits_{i,j>i,k>j} \mathbf{V}_{ijk} + \cdots + \mathbf{V}_{1,2,\ldots,n} \quad (26)$$

where $\mathbf{V}_i = \mathrm{Var}(\mathrm{E}[\mathbf{Z}|\mathbf{Y}_i])$,
$\mathbf{V}_{ij} = Var(\mathrm{E}[\mathbf{Z}|\mathbf{Y_i}, \mathbf{Y}_j]) - \mathbf{V}_i - \mathbf{V}_j$,
$\mathbf{V}_{ijk} = \mathrm{Var}(\mathrm{E}[\mathbf{Z}|\mathbf{Y_i}, \mathbf{Y_j}, \mathbf{Y}_k]) - \mathbf{V}_{ij} - \mathbf{V}_{jk} - \mathbf{V}_{ik} - \mathbf{V}_i - \mathbf{V_j} - \mathbf{V}_k$, etc.
Therefore,

$$\sum\nolimits_i \mathbf{SI}_i + \sum\nolimits_{i,j>i} \mathbf{SI}_{ij} + \sum\nolimits_{i,j>i,k>j} \mathbf{SI}_{ijk} + \cdots + \mathbf{SI}_{1,2,\ldots,n} = 1. \quad (27)$$

For measuring the total effect of all input variables, the total effect index is utilised [91], as shown in Eq. (28)

$$\mathbf{SI}_{Ti} = 1 - \mathrm{Var}(\mathrm{E}[\mathbf{Z}|\mathbf{Y}_1, \ldots, \mathbf{Y}_{i-1}, \mathbf{Y}_{i+1}, \ldots, \mathbf{Y}_n])/\mathrm{Var}(\mathbf{Z}). \quad (28)$$

The advantage of SA includes that it provides fine-grained information on individual and compound effects of input variables. The limitation of SA is linked with Monte Carlo, wherein it is a computationally exhaustive process requiring time and cost. MARS is utilised as a surrogate model in the present study to overcome this limitation.

Multivariate Adaptive Regression Splines (MARS)

The finite element modelling (in the case of computationally intensive simulation of repetitive nature) [55, 95–101] can be an alternate way where inefficient analytical solutions [92–94] are not possible. The surrogate modelling technique is employed in such intensive simulations to achieve computational efficiency. In the case of MARS relationship between input/output responses of the system is achieved by selecting samples based on some algorithms [102–104]. Instead of assuming the functional relationship between dependent and independent variables, here, essential function and set of coefficients are used to develop the times extracted from regression data. By employing MARS, significant dimensional input parameters problems can be obtained, otherwise difficult to solve. The forward and backward approach selects a set of basic functions for approximating the output response. Following steps are employed in MARS-based surrogate approach: step 1: initialisation with a simple model with constant basic function, step 2: addition of the basic functions thereby increasing complexity, step 3: checking with the pre-defined complexity, step 4: using backward approach, remove insignificant basic functions. The basic function of MARS [105] can be expressed as,

$$\mathbf{f}(\mathbf{x}) = \sum_{i=1}^{J} \boldsymbol{\alpha}_i Z_i^x(\mathbf{y}_n). \quad (29)$$

The approximation function is represented by $f(x)$. α_i represents the coefficients of expansion, whereas the multivariate spline basic functions are denoted by $Z_i^x(y_n)$. For dividing input space into J number of regions, the Eq. (29) becomes

$$\mathbf{f}(\mathbf{x}) = \boldsymbol{\alpha}_1, \quad (30)$$

where $\mathbf{Z}_i^x(\mathbf{y_1}, \mathbf{y_2}, \mathbf{y_3}, \ldots, \mathbf{y}_J) = 1$ for $i = 1$. In Eq. (30), the term α_1 is the intercept parameter. The basic function can be expressed as,

$$\mathbf{Z}_i^x(\mathbf{y}_n) = \prod_{n=1}^{n_i} [\mathbf{K}_{n_i}(\mathbf{y}_{m(n,i)} - \mathbf{Q}_{n,i})]_{\mathrm{Pr}}^h, \quad (31)$$

where n_i represents the interaction order,$K_{n_i} = \pm 1$,$y_{m(n,i)}$ denotes the mth variable,$1 \le m(n,i) \le j$, and $Q_{n,i}$ represents the knot location of corresponding variables. The dimension of input variables is defined by j, superscript x denotes the function, and l denotes the spline's order. The function $f(x)$ contains all the basic functions of ith sub-regions, while the multivariate spline basic function $\mathbf{Z}_i^x(\mathbf{y}_n)$ contains univariate spline basic function and $K_{n,i}$. 'Pr' represents the function as a truncated power function. The basic function may be in the following shapes

$$^{h}_{\mathrm{Pr}} = [\mathbf{K}_{n,i}(\mathbf{y}_{m(n,i)} - \mathbf{Q}_{n,i})]^h \ for\ [\mathbf{K}_{n,i}(\mathbf{y}_{m(n,i)} - \mathbf{Q}_{n,i})] < 0 \quad (32)$$

Otherwise

$$[\mathbf{K}_{n,i}(\mathbf{y}_{m(n,i)} - \mathbf{Q}_{n,i})] = 0. \quad (33)$$

Thus, all basic functions are expressed as

$$\mathbf{E} = \{[\mathbf{K}_{n,i}(\mathbf{y}_{m(n,i)} - \mathbf{Q}_{n,i})]^h_{\mathrm{Pr}}\}, \mathbf{Q} \in \{\mathbf{y}_{1m}, \mathbf{y}_{2m}, \mathbf{y}_{3m} \ldots\ldots \mathbf{y}_{Jm}\} \tag{34}$$

Stepwise linear regression is employed for forward propagation, but instead of using original input, it uses the function $\boldsymbol{E}$ and their product. For estimating $\boldsymbol{\alpha}_i$, the residual sum-of-square is minimised. Both forward and backward approaches are employed in MARS to determine the number of basic spline functions and their location. First, the basic spline function is over-fitted at each knot, then for removing insignificant knot, the modified cross-validation criteria are employed [106, 107].

The model uses a modified kind of criterion known as generalised cross-validation (GCV) to automatically screen the variables. For the appropriate spline basis functions, MARS picks the exact value and location of the given element in an onward or backward way. It over-fits the spline function to the defined knot's position. After that, using the generalised cross-validation criterion, the model removes the unneeded knots that contribute the least to the model. The knots that are not needed can be assessed using the lack-of-fit ($\mathbf{Z}$) criterion, which is represented as

$$\mathbf{Z} = G_c(k) = \frac{\frac{1}{h}\sum_{i=1}^{h}[\boldsymbol{Y}_i - \boldsymbol{Y}_k(x_i)]^2}{[1 - \frac{\tilde{c}(\tilde{k})}{n}]^2}, \tag{35}$$

where $\tilde{c}(\tilde{k}) = c(\tilde{k}) + C.(\tilde{k})$

'h' represents the total number of samples, $c(\tilde{k})$' represents the number of linearly independent basis functions, '$\tilde{k}$' represents the number of knots in the forward process, 'Y' represents the approximated function, and 'C' represents the basis function cost. The smoothness of the function is estimated by the cost function's value. Because 'C' is inversely proportional to the number of knots, when '$\tilde{k}$' is small, C is big, which results in a smooth estimation of the function.

The constructed metamodel is further validated by analysing the relative accuracy and the coefficient of determination (R^2) of the individual model. The formulation of the coefficient of determination is stated as

$$\mathbf{R}^2 = 1 - \frac{\sum_{i=1}^{n}(\mathbf{y}_i - \hat{\mathbf{y}}_i)^2}{\sum_{i=1}^{n}(\mathbf{y}_i - \bar{\mathbf{y}}_i)^2}. \tag{36}$$

Here, y_i,$\hat{y}_i$ and $\bar{y}_i$ signifies the actual model, predicted model and mean of actual data. In Eq. (57), it is assumed that all the parameters are influential in evaluating the model's efficiency. The relative accuracy of the model is evaluated as

Table 3 HMGS shells material properties

	Material properties	E (GPa)	ν	ρ (kg/m^3)
FGM	Ceramic	151	0.3	3000
	Metal	70	0.25	2707
Soft core		0.85	0.42	1000
Laminated composite		19.3	0.25	2600

$$\boldsymbol{RA}(\%) = 1 - \left|\frac{\boldsymbol{J}(\boldsymbol{x})_{\text{predicted}} - \boldsymbol{J}(\boldsymbol{x})_{\text{actual}}}{\boldsymbol{J}(\boldsymbol{x})_{\text{predicted}}}\right|. \tag{37}$$

$\mathbf{J}(\mathbf{x})_{\text{actual}}$ and $\mathbf{J}(\mathbf{x})_{\text{predicted}}$ are the FE response and corresponding predicted response of the MARS model, respectively. The current model is designed with input variables as mentioned in Table 3. The parameters are chosen based on the number of layers and six different types of shell geometries.

$$\mathbf{RMSE} = \frac{\sqrt{\sum_{i=1}^{n} ||\mathbf{y}_i - \hat{\mathbf{y}}_i||^2}}{n}. \tag{38}$$

For numerical predictions, the root mean square error (RMSE) is regarded as an excellent general-purpose error metric. Because RMSE is scale dependent, it should only be used to evaluate prediction errors of different models or model configurations for a single variable, not between variables. It is a metric for determining how well a regression line fits the data points. The following is the formula for computing RMSE.

Results and Discussion

The present study investigates the effect of various random input parameters (like material properties and geometric variations) for the first three natural frequencies response of HMGS shell structures. The sensitivity analysis is performed to identify the effect of each random input parameter on the global response of the structure. The probabilistic results are obtained from the efficient MARS integrated finite element (FE) framework. Figure 4 illustrates the flow diagram for sensitivity analysis for stochastic natural frequency of hybrid multi-functionally graded sandwich (HMGS) shells. The validation of the present model is accomplished in two ways. First, the deterministic model is validated by comparing the FE code with past literature. Second, the stochastic surrogate-based MARS model is validated with traditional

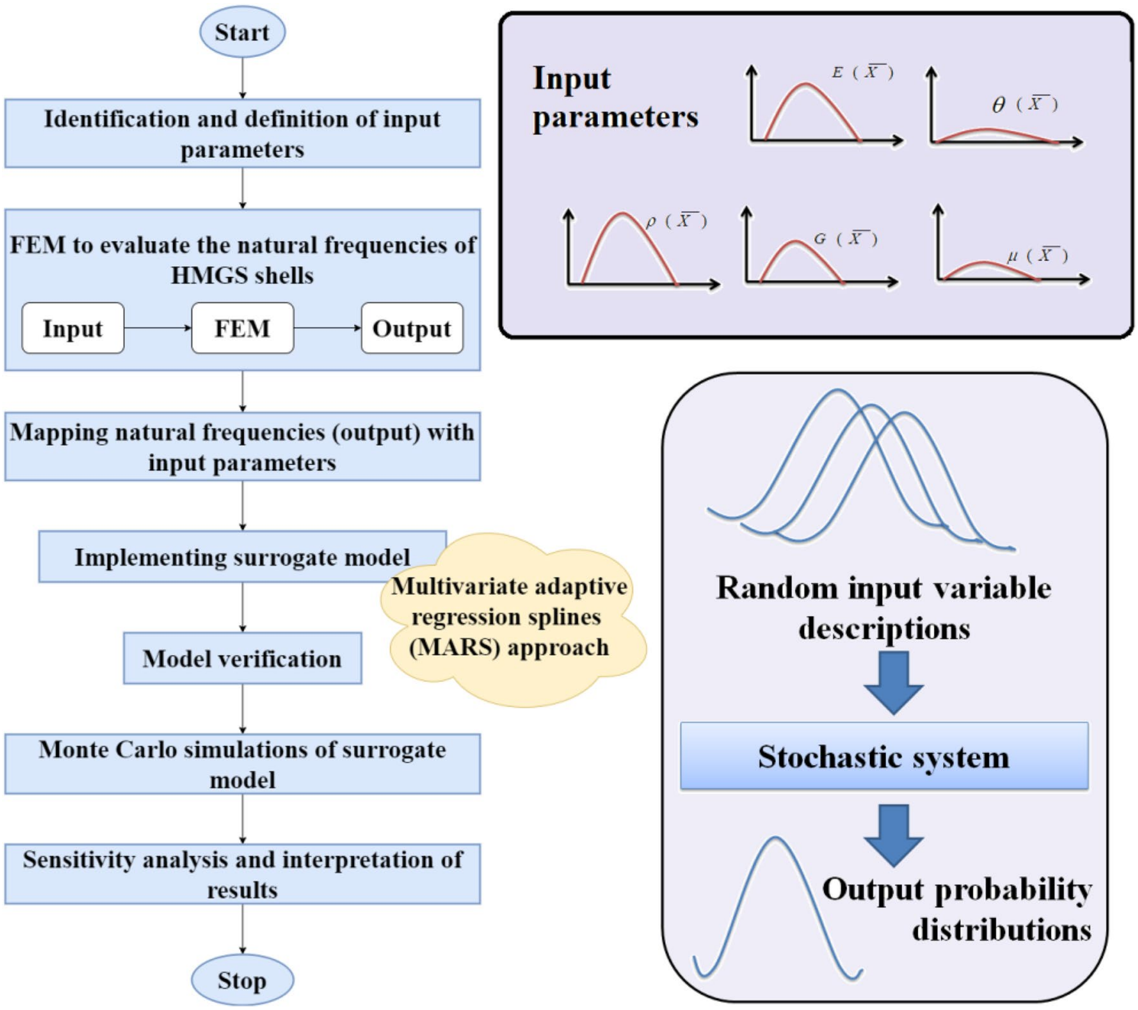

Fig. 4 Flow diagram for sensitivity analysis for stochastic natural frequency of hybrid multi-functionally graded sandwich (HMGS) shells

MCS-based results. In the present study, elliptical paraboloid, cylindrical, hyperbolic paraboloid, and spherical shell (Fig. 1) of HMGS structures are studied for their dynamic response. The basic materials of HMGS shells are FG-based material of metal and ceramic mixture (aluminium is considered as metal and zirconia as ceramic) [108], the low-density soft core of foam material, and laminated composite (material properties presented in Table 3) [109]. Table 4 shows the first natural frequency for various mesh sizes (6 × 6, 8 × 8, 10 × 10) and for different values of power-law exponent (x) compared with the results presented by Zhao and Liew [39]. The results obtained demonstrate an acceptable approximation of the present study and with the results of Zhao and Liew [39]. Furthermore, mesh convergence of hybrid FG-sandwich cylindrical shells is conducted (refer to Fig. 5). From this mesh convergence study, the optimal mesh size is selected. To reduce computational time 6 × 6 mesh size is considered. Also, it is found that (from Table 3) the percentage of error for other mesh sizes is comparatively higher than that of 6 × 6. The FG cantilever plate of 6 × 6 mesh size is considered for deterministic FE analysis, which provides satisfactory results, leading to 36 elements and 133 nodes. The deterministic result obtained is thus validated with that of results available in previous literature [110–112], as presented in Tables 5 and 6. There seems to be a good agreement for several cases of t/L ratio and power-law exponent (p) and for various shell geometries. The thickness of the plate is represented by "t", and "l" represents the length

Table 4 Validation of mesh convergence for FNF of functionally graded shells subjected to free vibration

Power law (x)	Zhao and Liew [39]	Present FEM		
		6 × 6	8 × 8	10 × 10
0	1.3666	1.3608	1.3449	1.2356
1	1.1893	1.1792	1.1641	1.1038
10	1.0404	1.0222	1.0102	0.9566

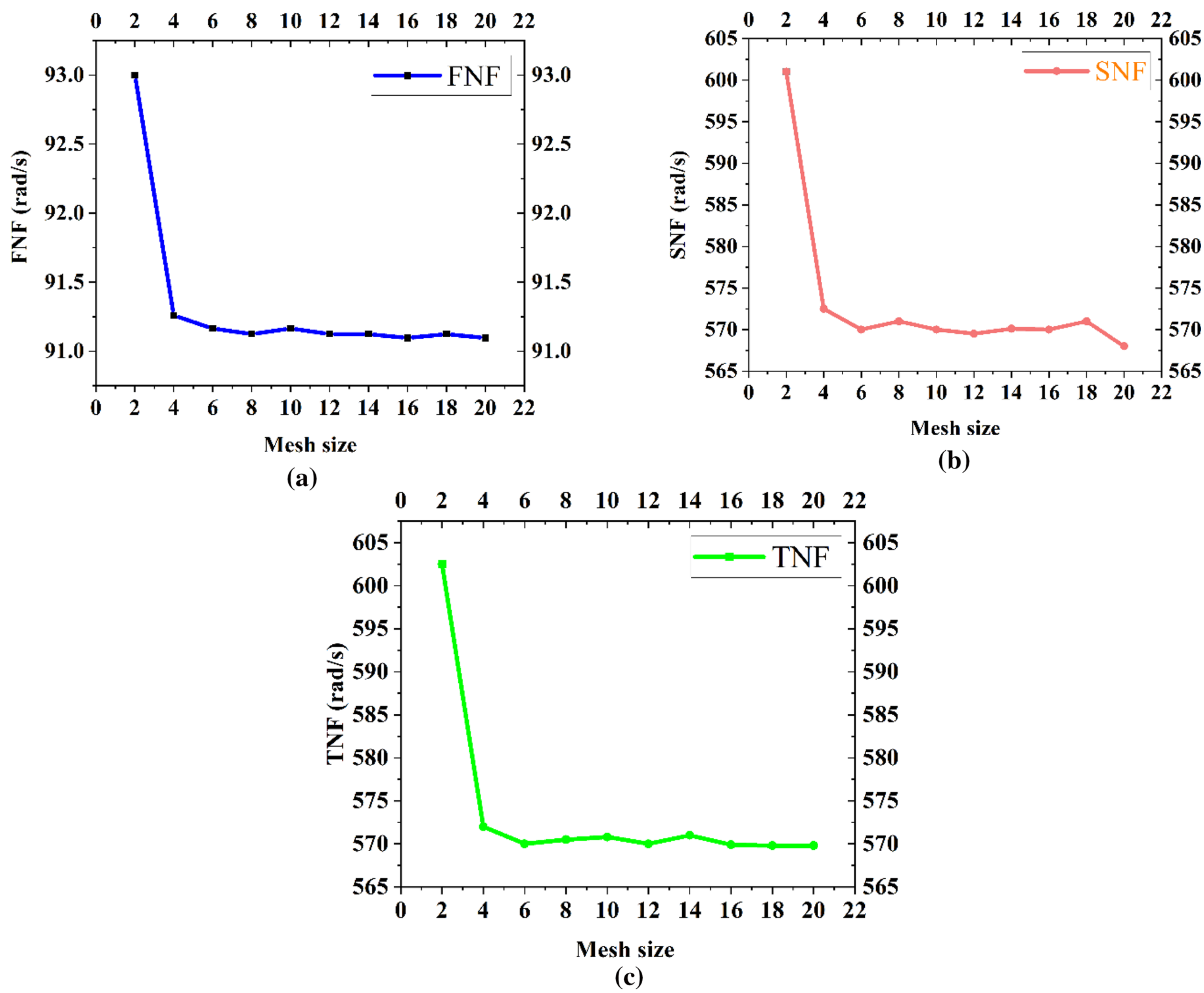

Fig. 5 Mesh convergence study of FE analysis of first three natural frequencies for different mesh size

Table 5 Validation for FNF of functionally graded square plate subjected to free vibration

p	*t/L*	Baferani et al. [110]	Ta and Noh [111]	Present study
0	0.1	0.1134	0.1134	0.1139
	0.2	0.4154	0.4152	0.4159
1	0.1	0.0891	0.0869	0.0883
	0.2	0.3299	0.3205	0.3261
2	0.1	0.0819	0.0788	0.0797
	0.2	0.3016	0.2897	0.3004

of the plate. Once the FE code is verified, the natural frequencies of an elliptical paraboloid, cylindrical, hyperbolic paraboloid, and spherical-shaped HMGS shells with different cases (total six cases) are investigated.

As per industry standards, for the present analysis, the probabilistic variation of random input parameters is considered as $C = 10\%$ concerning the respective deterministic nominal values for obtaining the numerical results [113]. Depth-wise uncertainty is contemplated for variations of material properties (in the z-direction) as it is critical in hybrid multi-functionally graded sandwich structures. The computational efficiency is achieved by employing the MARS as the surrogate model in conjunction with FE code. The predictability of the result obtained through MARS is validated with the results of direct FE simulation through scatter plot. To reduce the computational cost, the surrogate model is formed by considering sample sizes of 256, 512, and 1024. For convergence study, some of the parametric analyses are performed; they are R-squared value, root mean square error (RMSE), mean absolute error (MAE), and mean square error (MSE), as illustrated in Table 7a–d. It is

Table 6 Validation for various shell geometries and various power-law exponent on FNF of FG shells having ($\boldsymbol{E}_c = 380$ GPa, $\boldsymbol{\rho}_c = 3800$ kg/m3, $\boldsymbol{E}_m = 70$GPa, $\boldsymbol{\rho}_m = 2702$ kg/m3, $\nu = 0.3$)

Types of shells		$p=1$	$p=5$	$p=10$
Cylindrical ($R_x=5$, $R_y=$Infinite)	Sayyad et al. [112]	0.16546	0.14013	0.13458
	Present study	0.16543	0.14011	0.13455
Spherical ($R_x=R_y=5$)	Sayyad et al. [112]	0.16748	0.14142	0.13574
	Present study	0.16744	0.14139	0.13570
Hyperbolic paraboloid ($R_x=5$, $R_y=-5$)	Sayyad et al. [112]	0.16452	0.13955	0.13400
	Present study	0.16449	0.13950	0.13396
Elliptical paraboloid ($R_x=5$, $R_y=7.5$)	Sayyad et al. [112]	0.16669	0.14091	0.13530
	Present study	0.16963	0.14088	0.13527
Plates ($R_x=R_y=$infinite)	Sayyad et al. [112]	0.16521	0.14014	0.13458
	Present study	0.16517	0.14011	0.13457

perceived that for sample size 1024, the percentage error is comparatively less than others (refer to Table 7a–d). The probability density function (PDF) plots (Fig. 6a–f) show the predicted outputs obtained while implementing the MARS surrogate model for different sample sizes (256, 512, and 1024) and the output obtained from the original MCS for the sample size of 10,000.

MCS is a computing technique for the (typically approximate) solution of mathematical problems that employ random samples as its foundation. It is one of the most intriguing computational device for performing statistical inference in the field of stochastic analysis. Many fascinating models have incredibly complicated structures that are difficult to solve using typical methods. The posterior probability distribution encodes all information on which inference can be made within the bounds of the output quantity of interest. We can characterise these distributions and calculate expectations under them using MCS. Thus, it can be inferred that although MCS provides a robust output in probabilistic regime its one disadvantage is the consumption of time and computational efficiency. It is mitigated by the utilization of MARS as the surrogate model.

It is reviewed that the predictions for the 1024 sample size are satisfactory compared to sample sizes 256 and 512. After that, the result obtained by MARS is compared with the conventional MCS for a converged sample size of 1024, as depicted in Fig. 7a–f. The scatter plot for the same sample size, 1024 (refer to Fig. 6-a–f), portrays the minor deviation. Therefore, a sample size of 1024 is considered for further stochastic analysis. Both Figs. 6 and 7 show the excellent forecasting capability of the MARS model irrespective of the shell geometries and generate enough assurance on the MARS-based stochastic analysis for all cases.

The present analysis considers the depth-wise varying framework (in 'z-direction') for four shell geometries of six structural forms. It is noted that the variation in material properties occurs throughout the thickness. The uncertainty in material properties is considered for stochastic analysis. Sensitivity analysis is performed for assessing the relative significance of the stochastic material properties (like Young's modulus (E), shear modulus (G), Poisson's ratio (μ), mass density (ρ) and stochastic geometric configuration (ply-orientation angle (θ)) on the free vibration response of different shell geometries for several structural forms. The structures are subjected to free vibration to determine the most significant parameters in the global response of the structure. In the case of HMGS, sensitivity analysis is essential for the optimal design of the structures. It is significant to attribute for controlling of various random input variables, arising during the manufacturing process and different stages of operations. Figure 8a–f presents the sensitivity analysis of elliptical paraboloid, cylindrical, hyperbolic paraboloid, and spherical-shaped HMGS shells. Figure 8a represents the sensitivity analysis of HMGS shells for various geometries for case 1. In this case (case 1), hybrid structures are designed such that the upper facesheet is composed of the laminated composite while the lower facesheet is constructed of FGM, and in between, there is a soft core. From Fig. 8a, shows that for the cylindrical shell, ρ is obtained as the most sensitive parameter followed by E_1, E_2 and θ while other parameters are found to be the least significant. For spherical and elliptical paraboloid shells, ρ is the most sensitive parameter, while E_1, E_2, θ, G_{12} show the moderate effect, and other parameters have negligible effect. In hyperbolic paraboloid shells, θ is the most sensitive parameter followed by ρ. At the same time E_1, E_2 and G_{12} show moderate effects. Figure 8b represents the sensitivity analysis of HMGS shells for various geometries for case 2. In this case (case 2), hybrid structures are designed such that both the facesheets are of FGM, and in the middle, there is a soft core. From Fig. 8b, it is noted that for all shell geometries, ρ is the most sensitive parameter followed by E_1 and G_{12}. In contrast, E_2 and υ have moderate effects, whereas other parameters are obtained as the least significant parameters. Figure 8c represents the sensitivity analysis of HMGS shells for various geometries for case 3. In this case (case 3), hybrid structures are designed to

Table 7 Error analysis for the first three random NF (rad/s) of HMGS (**a**) cylindrical shell, (**b**) spherical shell, (**c**) elliptical paraboloid shell, (**d**) hyperbolic paraboloid shell for 256, 512, and 1024 sample-sized FE-MARS approaches of compound variation arbitrarily selected input parameters ($C = 10\%$)

Cases	$N = 256$			$N = 512$			$N = 1024$		
	FNF	SNF	TNF	FNF	SNF	TNF	FNF	SNF	TNF
(a)									
Case 1									
RMSE	0.27062	1.02989	1.57223	0.27278	0.96297	1.56298	0.25886	0.88248	1.47048
R-squared	0.94724	0.74404	0.95358	0.94854	0.81969	0.95567	0.95283	0.83457	0.95986
MSE	0.07383	1.07503	2.48516	0.07445	0.93354	2.44678	0.06718	0.77963	2.16884
MAE	0.22785	0.50190	0.21416	0.22620	0.42270	0.20990	0.21703	0.40611	0.20007
Case 2									
RMSE	0.71208	1.64218	4.40801	0.61823	1.46977	3.77646	0.62854	1.33839	3.86534
R-squared	0.65865	0.58744	0.65986	0.75652	0.73594	0.75146	0.78651	0.76329	0.79353
MSE	0.50942	2.70109	19.5202	0.38536	2.17218	14.2920	0.39557	1.80350	14.9489
MAE	0.58108	0.63994	0.58013	0.45943	0.51262	0.45588	0.49227	0.48517	0.49630
Case 3									
RMSE	0.83521	2.02008	5.51315	0.74882	1.82300	4.63762	0.80116	1.75604	4.73560
R-squared	0.68918	0.70969	0.63415	0.71284	0.72032	0.71218	0.72174	0.76814	0.74047
MSE	0.70813	4.13418	30.7880	0.56635	3.33671	21.7113	0.64341	3.08685	22.4586
MAE	0.55613	0.98772	0.60204	0.49446	0.84101	0.49533	0.52649	0.78209	0.50914
Case 4									
RMSE	0.28948	0.66114	1.74458	0.25268	0.63240	1.51357	0.25368	0.63786	1.55392
R-squared	0.97471	0.96879	0.97605	0.98104	0.97376	0.98009	0.98330	0.97717	0.98299
MSE	0.08457	0.43757	3.06960	0.06434	0.40197	2.29444	0.06447	0.40771	2.42194
MAE	0.15815	0.17580	0.15392	0.12847	0.15059	0.12997	0.13740	0.16183	0.14045
Case 5									
RMSE	0.70155	1.60054	4.42257	0.64006	1.40525	4.05580	0.59142	1.33834	3.68413
R-squared	0.63740	0.55426	0.62421	0.74875	0.72472	0.72810	0.75975	0.73480	0.74975
MSE	0.49511	2.58069	19.6605	0.41001	1.98515	16.4826	0.35031	1.79227	13.5873
MAE	0.60215	0.66414	0.61269	0.50121	0.52189	0.52015	0.48834	0.51368	0.49925
Case 6									
RMSE	0.37229	0.74353	2.30880	0.34960	0.76630	2.10203	0.31812	0.70067	1.97544
R-squared	0.50208	0.53679	0.50361	0.56330	0.50894	0.59110	0.71772	0.70739	0.71785
MSE	0.13974	0.56644	5.37404	0.12297	0.58798	4.43276	0.10144	0.49288	3.91145
MAE	0.70301	0.66738	0.70200	0.65877	0.70055	0.63801	0.61814	0.62584	0.61803
(b)									
Case 1									
RMSE	1.68943	0.65326	2.61650	1.38731	0.64715	2.44016	1.26221	0.61573	2.38091
R-squared	0.46245	0.91994	0.87396	0.70958	0.93220	0.89911	0.71462	0.92431	0.90740
MSE	2.87250	0.42987	6.86583	1.94298	0.41986	5.97406	1.59635	0.37964	5.67233
MAE	0.72791	0.28147	0.35424	0.53597	0.25958	0.29984	0.53400	0.27472	0.31991
Case 2									
RMSE	1.60504	1.92150	5.10003	1.36991	1.60759	4.67967	1.30630	1.49299	4.45186
R-squared	0.56562	0.53159	0.60165	0.74613	0.74018	0.72010	0.75207	0.75601	0.72995
MSE	2.59564	3.75177	26.2803	1.88719	2.60949	21.9393	1.70716	2.23295	19.8433
MAE	0.65601	0.67834	0.62779	0.49049	0.50887	0.52712	0.50719	0.49282	0.51865
Case 3									
RMSE	2.36138	1.54690	7.04198	2.05507	1.69533	5.67956	2.18061	1.56858	5.81432
R-squared	0.49011	0.58992	0.53600	0.58227	0.59109	0.55986	0.70840	0.75075	0.74635
MSE	5.67914	2.40377	50.0622	4.22515	2.87729	32.2866	4.76828	2.46432	33.8500
MAE	1.02993	0.64003	0.94323	0.83499	0.63938	0.67767	0.86548	0.62324	0.70904
Case 4									
RMSE	0.67491	0.78623	3.59460	0.65213	0.71775	3.43357	0.62456	0.72451	3.25762

Table 7 (continued)

Cases	$N=256$			$N=512$			$N=1024$		
	FNF	SNF	TNF	FNF	SNF	TNF	FNF	SNF	TNF
R-squared	0.96418	0.96228	0.90022	0.97357	0.97548	0.92757	0.97132	0.97169	0.92561
MSE	0.45800	0.61919	13.0084	0.42560	0.51981	11.8320	0.39056	0.52549	10.6980
MAE	0.18831	0.19305	0.31259	0.16222	0.15583	0.26864	0.16918	0.16804	0.26939
Case 5									
RMSE	1.53868	1.81919	5.00601	1.34594	1.53760	4.37061	1.25098	1.43883	4.15787
R-squared	0.54986	0.52848	0.59824	0.74728	0.73037	0.72803	0.73723	0.75016	0.72525
MSE	2.37410	3.33899	25.7593	1.81236	2.40187	19.2130	1.56964	2.07752	17.3008
MAE	0.66776	0.67962	0.62866	0.50217	0.51359	0.52090	0.51199	0.49896	0.52347
Case 6									
RMSE	1.06815	0.91946	3.01313	0.92289	0.98141	2.78438	0.82373	0.88253	2.59699
R-squared	0.28059	0.56300	0.41620	0.46607	0.47635	0.50104	0.76864	0.69686	0.68036
MSE	1.14849	0.85546	9.16978	0.85411	0.96564	7.80489	0.67918	0.78154	6.75180
MAE	0.84239	0.65892	0.75765	0.72875	0.72244	0.70406	0.65614	0.63481	0.64756
(c)									
Case 1									
RMSE	1.53232	1.64216	2.58273	1.40637	1.41344	2.31698	1.25633	1.37969	2.18968
R-squared	0.68378	0.84128	0.87312	0.79511	0.84924	0.90717	0.79543	0.85892	0.91482
MSE	2.36726	2.70084	6.71840	2.00438	2.35542	5.44226	1.58085	1.90714	4.81696
MAE	0.55620	0.39736	0.35425	0.44908	0.38643	0.28398	0.45146	0.37512	0.30752
Case 2									
RMSE	2.50659	2.75321	4.95217	1.94572	2.55320	4.45534	1.77807	2.31208	4.32709
R-squared	0.40796	0.61449	0.68408	0.73033	0.74376	0.75958	0.74887	0.74778	0.76217
MSE	6.42914	7.68851	24.6329	3.78672	6.54164	19.9219	3.16230	5.35141	18.7403
MAE	0.76530	0.61732	0.56131	0.51865	0.50449	0.48860	0.50086	0.50144	0.48719
Case 3									
RMSE	2.62088	2.93466	6.93521	2.18777	3.20558	5.44550	2.22739	2.78288	5.24440
R-squared	0.48064	0.45756	0.20364	0.61319	0.47983	0.60056	0.78974	0.68347	0.67306
MSE	6.96496	8.68236	48.4315	4.79695	10.3152	29.7354	4.96744	7.78120	27.5520
MAE	0.97240	0.73357	0.88907	0.76446	0.71925	0.63115	0.76119	0.64502	0.61315
Case 4									
RMSE	1.10305	1.77950	3.88194	1.04817	1.71083	3.57035	1.02511	1.57676	3.19178
R-squared	0.94714	0.91693	0.88443	0.95149	0.94028	0.92841	0.96857	0.94290	0.93702
MSE	1.22740	3.18396	15.1311	1.10016	2.93152	12.8368	1.05269	2.48778	10.2218
MAE	0.22876	0.28628	0.33923	0.19566	0.24397	0.26648	0.20331	0.23851	0.25014
Case 5									
RMSE	2.24322	2.75178	5.86183	1.82686	2.46952	4.50359	1.70443	2.21214	4.25710
R-squared	0.47299	0.58442	0.50190	0.73308	0.73381	0.72440	0.74522	0.74466	0.74448
MSE	5.11035	7.70181	34.5376	3.35290	6.10244	20.3080	2.91356	4.89978	18.1471
MAE	0.72339	0.64314	0.70485	0.51387	0.51531	0.52415	0.50362	0.50499	0.50533
Case 6									
RMSE	1.21935	1.79458	3.08418	1.28840	1.57979	2.96835	1.18983	1.51357	2.58292
R-squared	0.55724	0.46369	0.41970	0.66177	0.56353	0.52556	0.70798	0.69759	0.69309
MSE	1.49577	3.24320	9.59065	1.66253	2.50732	8.81751	1.42382	2.29689	6.68335
MAE	0.66366	0.72913	0.75270	0.73247	0.66003	0.76270	0.66440	0.63273	0.63680
(d)									
Case 1									
RMSE	1.03064	0.79370	3.27037	0.95991	0.77640	3.34865	0.91392	0.77217	3.29490
R-squared	0.77280	0.86888	0.86482	0.84427	0.87508	0.87116	0.84912	0.88854	0.88956
MSE	1.07388	0.63445	10.7260	0.92303	0.60519	11.2765	0.83880	0.59688	10.8856

Table 7 (continued)

Cases	$N=256$			$N=512$			$N=1024$		
	FNF	SNF	TNF	FNF	SNF	TNF	FNF	SNF	TNF
MAE	0.46806	0.36062	0.36723	0.39308	0.33736	0.35530	0.38810	0.34788	0.36066
Case 2									
RMSE	1.78656	1.90737	7.13913	1.38893	1.50400	5.84191	1.28642	1.41817	5.50677
R-squared	0.41187	0.48537	0.43366	0.69043	0.75611	0.66081	0.70892	0.76094	0.70770
MSE	3.26796	3.78124	51.4598	1.94000	2.27270	34.2494	1.65587	2.01960	30.3439
MAE	0.75914	0.69979	0.74818	0.54644	0.49218	0.58042	0.54779	0.48698	0.54026
Case 3									
RMSE	3.98522	3.49566	10.8485	3.34051	3.23138	8.05620	2.99397	2.87747	9.19044
R-squared	0.43456	0.50778	0.50829	0.50326	0.58532	0.62559	0.69230	0.74727	0.73508
MSE	15.9836	12.3556	118.057	11.2513	10.5295	65.2207	9.06063	8.28182	84.7499
MAE	1.15402	1.03336	1.03435	1.01396	0.93781	0.83678	0.83866	0.80770	0.81429
Case 4									
RMSE	1.36891	0.79078	5.37971	1.26341	0.78564	4.92776	1.15102	0.75603	4.59392
R-squared	0.84300	0.96073	0.84242	0.88410	0.96793	0.89544	0.88491	0.96800	0.90501
MSE	1.90419	0.62623	29.0377	1.60207	0.61821	24.3392	1.32732	0.57207	21.1111
MAE	0.39222	0.19743	0.39233	0.33996	0.17605	0.32240	0.33847	0.18122	0.30787
Case 5									
RMSE	1.73192	1.68096	6.10536	1.32344	1.48330	5.77580	1.24008	1.36992	5.34286
R-squared	0.40749	0.57263	0.52198	0.69378	0.73476	0.63657	0.69921	0.75010	0.69399
MSE	3.01658	2.82995	37.5740	1.76501	2.20543	33.6077	1.54224	1.88545	28.5963
MAE	0.76820	0.65046	0.68217	0.55005	0.51403	0.60005	0.55484	0.49826	0.55233
Case 6									
RMSE	0.90333	0.88678	3.64396	0.87190	0.90018	3.59568	0.77590	0.83925	3.28453
R-squared	0.41799	0.53063	0.48284	0.56241	0.56930	0.59466	0.71518	0.76640	0.75045
MSE	0.82528	0.79578	13.4181	0.76184	0.81220	12.9659	0.60262	0.70586	10.8262
MAE	0.81133	0.68023	0.77771	0.79639	0.72710	0.77563	0.69397	0.65733	0.69025

make both the facesheets composed of laminated composite, keeping a soft core in the middle. On careful observation of Fig. 8c, it is found that for cylindrical shell ρ and θ are obtained as the most sensitive parameter, followed E_1 and E_2, while other parameters are obtained as the least significant. In contrast, ρ and E_1 (for spherical and elliptical paraboloid shells) show the maximum sensitivity followed by θ, G_{12}, and E_2, keeping other parameters having minor effects. In hyperbolic paraboloid shells,θ is obtained as the most sensitive parameter, followed by ρ. At the same time, E_1, E_2, and G_{12} show moderate effects. Figure 8d represents the sensitivity analysis of HMGS shells for various geometries for case 4. In this case (case 4), hybrid structures are designed to construct both the facesheet of FGM and laminated composite keeping the soft core in the middle. It is observed in Fig. 8d that for all the shell geometries, ρ predicts the highest sensitivity pursued by E_1, E_2, and G_{12}. In contrast, other parameters are observed to be the least significant parameters. Figure 8e represents the sensitivity analysis of HMGS shells for various geometries of case 5. In this case (case 5), hybrid structures are designed so that both the facesheets are FGM, and the middle core is laminated composite. Figure 8e shows that for all the shell geometries, ρ predicts the highest sensitivity corresponding to the fundamental natural frequencies. It is followed by E_1, E_2 and G_{12}, while others are found to be the least significant parameters. Figure 8f represents the sensitivity analysis of HMGS shells for various geometries of case 6. In this case (case 6), hybrid structures are designed so that both the facesheets are laminated composite and FGM's middle core. Figure 8f illustrates that for all the shell geometries, ρ predicts the highest sensitivity. It is followed by E_1, E_2, and G_{12}, whereas other parameters are comparatively less significant.

Conclusions

With the increasing attention to have multi-functionality in advanced structures, the necessity of sensitivity analysis corresponding to multiple response quantities simultaneously and to propose a unified sensitivity analysis framework has become apparent from the viewpoint of effective computational modelling and manufacturing quality

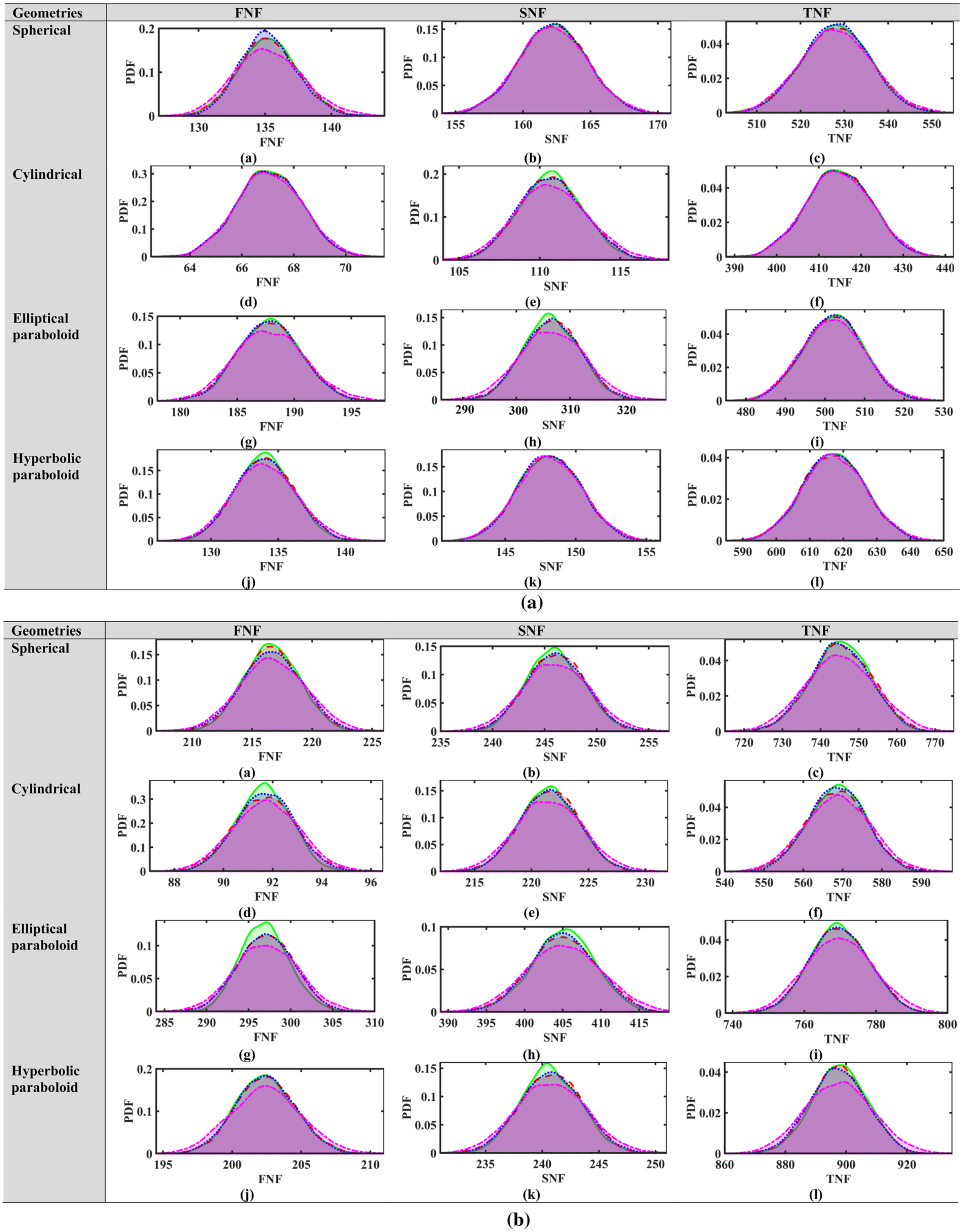

Fig. 6 **a** PDF plots of the first three random NF(rad/s) for **a** case 1, **b** case 2 **c** case 3 **d** case 4 **e** case 5 and **f** case 6 using the MARS approach depict the outcome of compound source-uncertainties of random input parameters considering stochasticity "C" = 10%. The details are furnished at the start of Sect. 3. Here represents $N = 256_{\mathrm{MARS}}$, represents $N = 512_{\mathrm{MARS}}$, represents $N = 1024_{\mathrm{MARS}}$ and represents $N = 10000_{\mathrm{MCS}}$

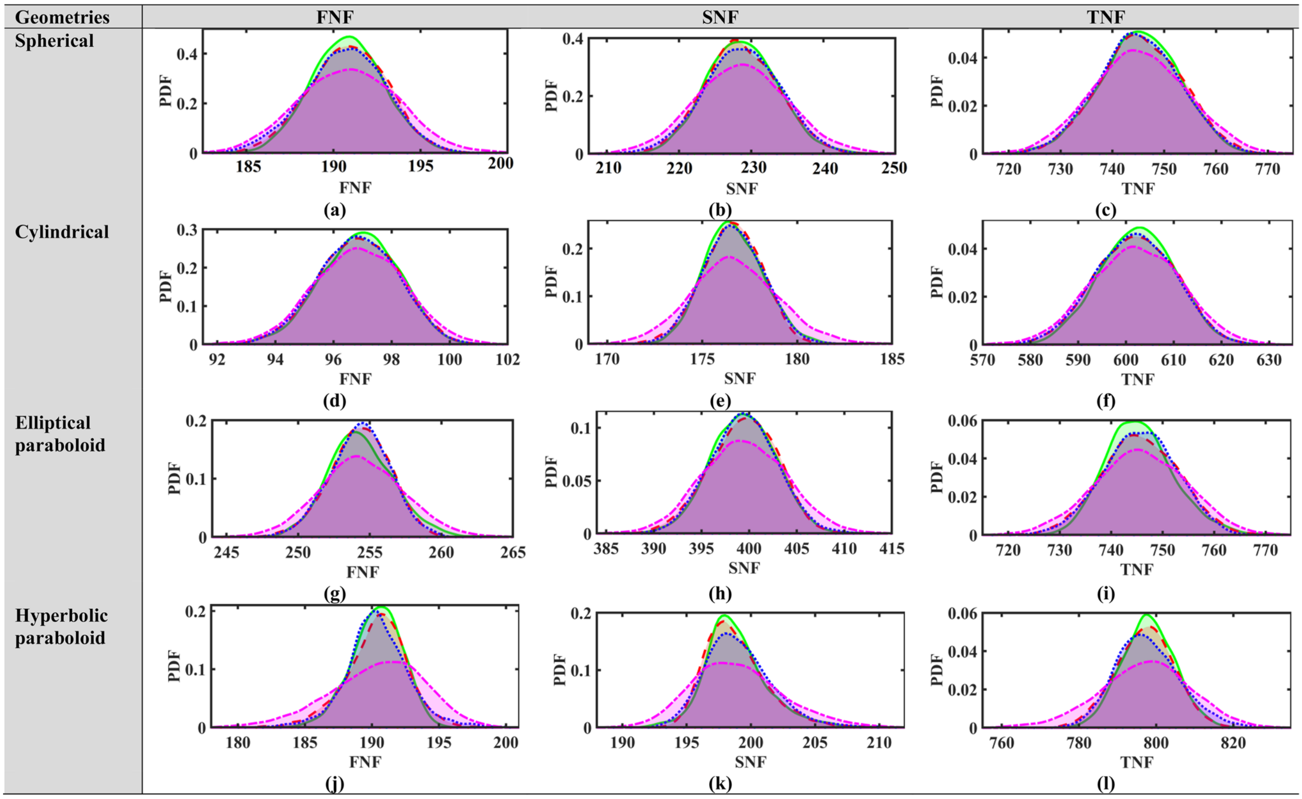

(c)

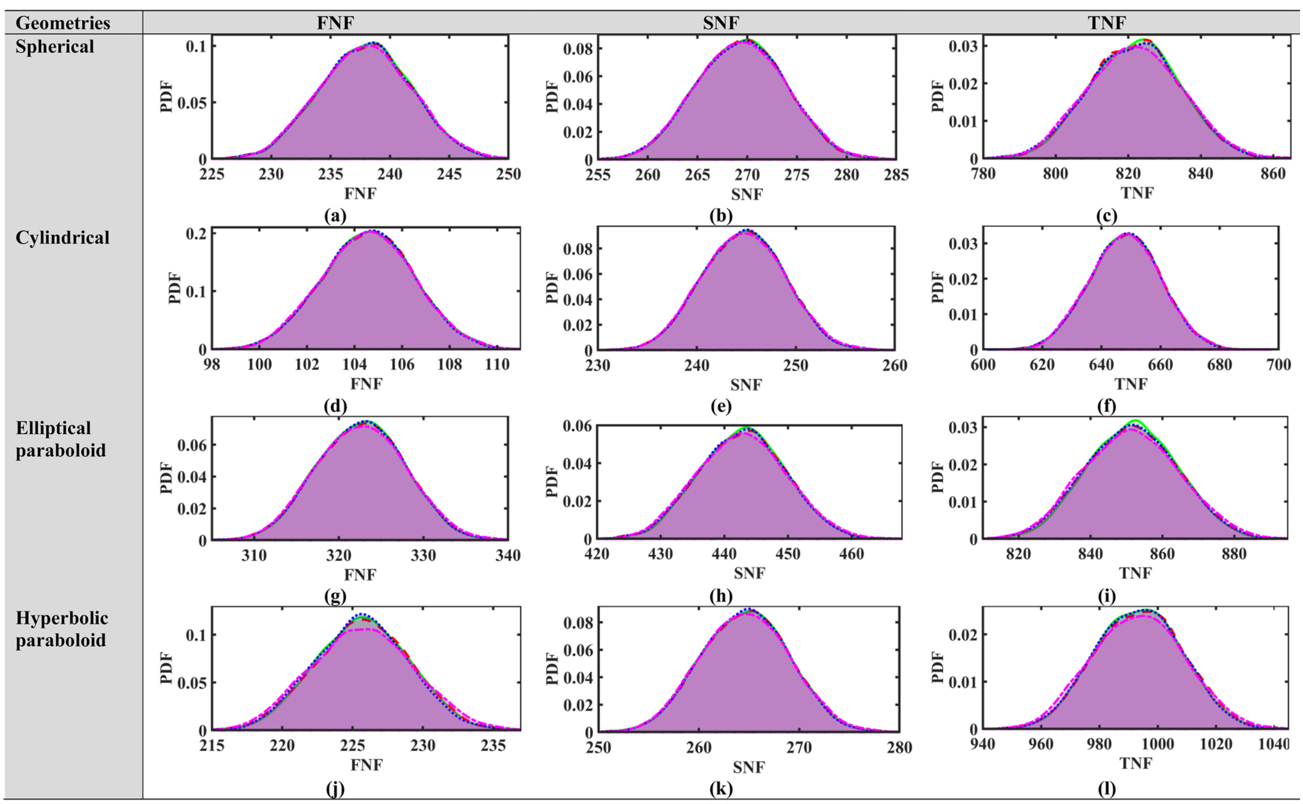

(d)

Fig. 6 (continued)

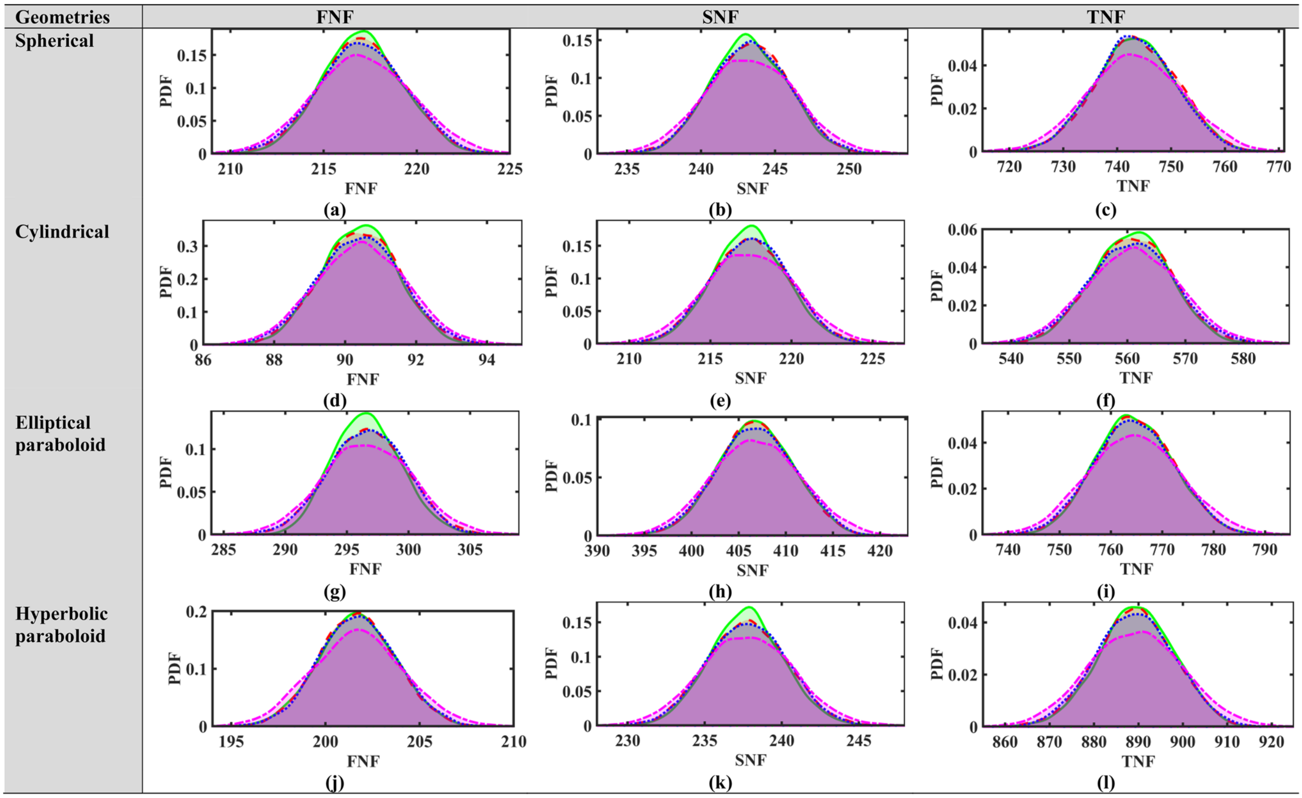

(e)

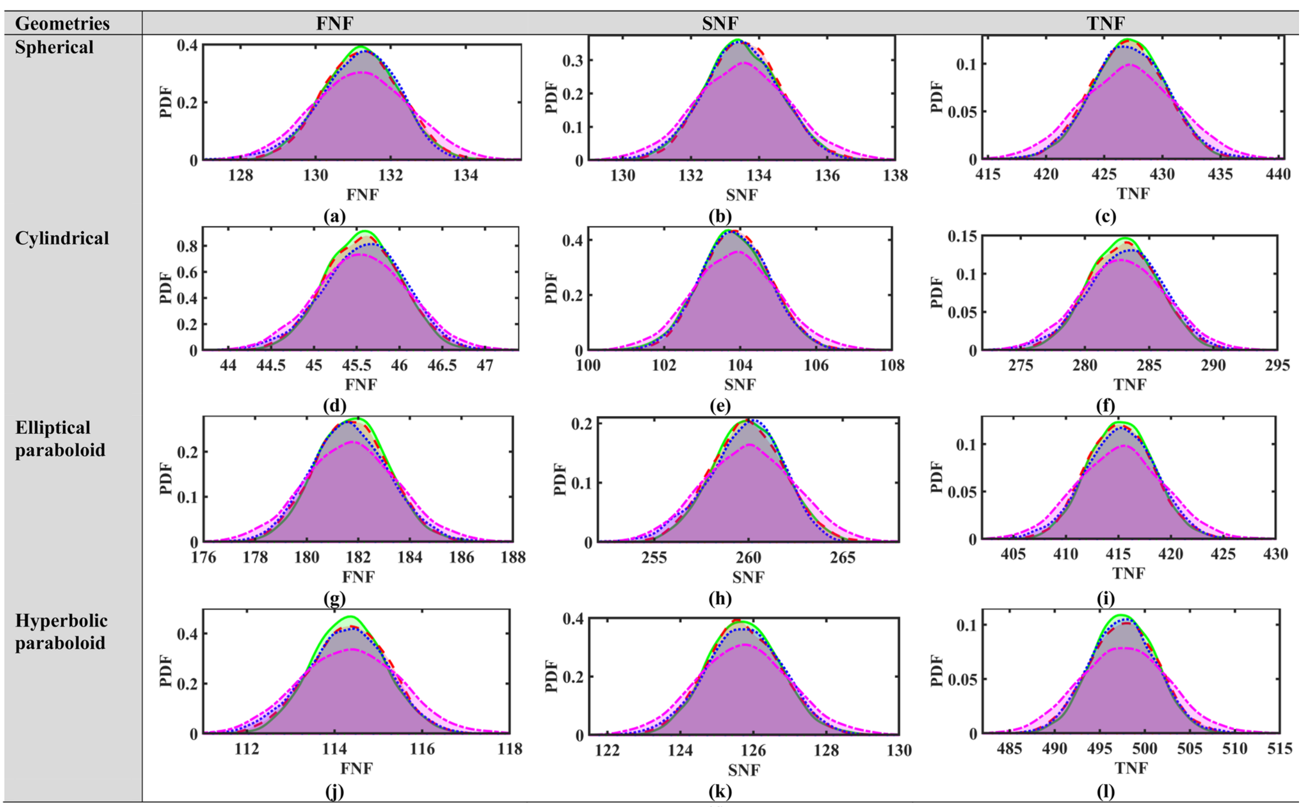

(f)

Fig. 6 (continued)

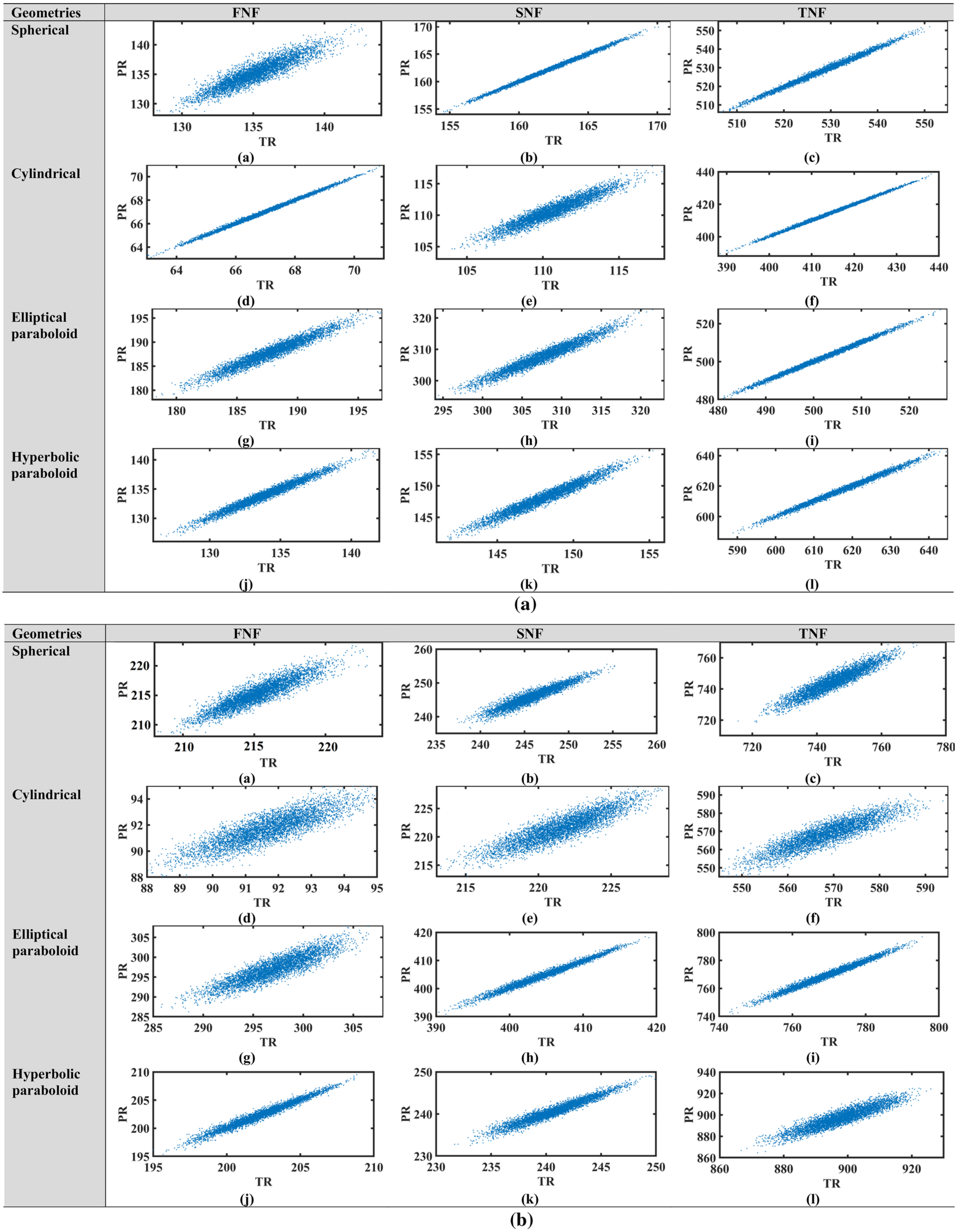

Fig. 7 Scatter plots of the first three random NF (rad/s) for **a** case 1, **b** case 2, **c** case 3, **d** case 4, **e** case 5 and **f** case 6 using MARS-MCS approach (1024 samples) and full-scale FE-MCS approach depicting the outcome of compound source-uncertainties of random input parameters considering stochasticity "*C*" = *10%*. Here *TR* true response and *PR* predicted response

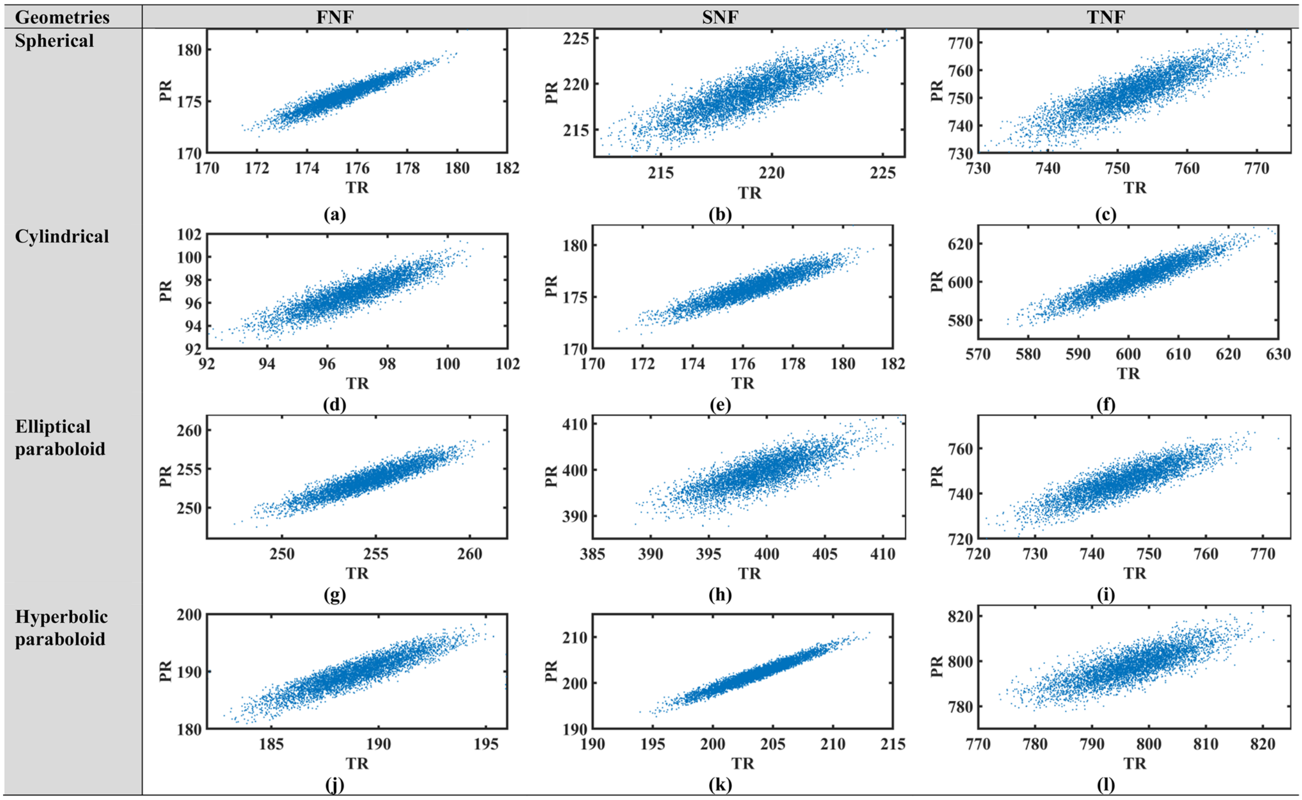

(c)

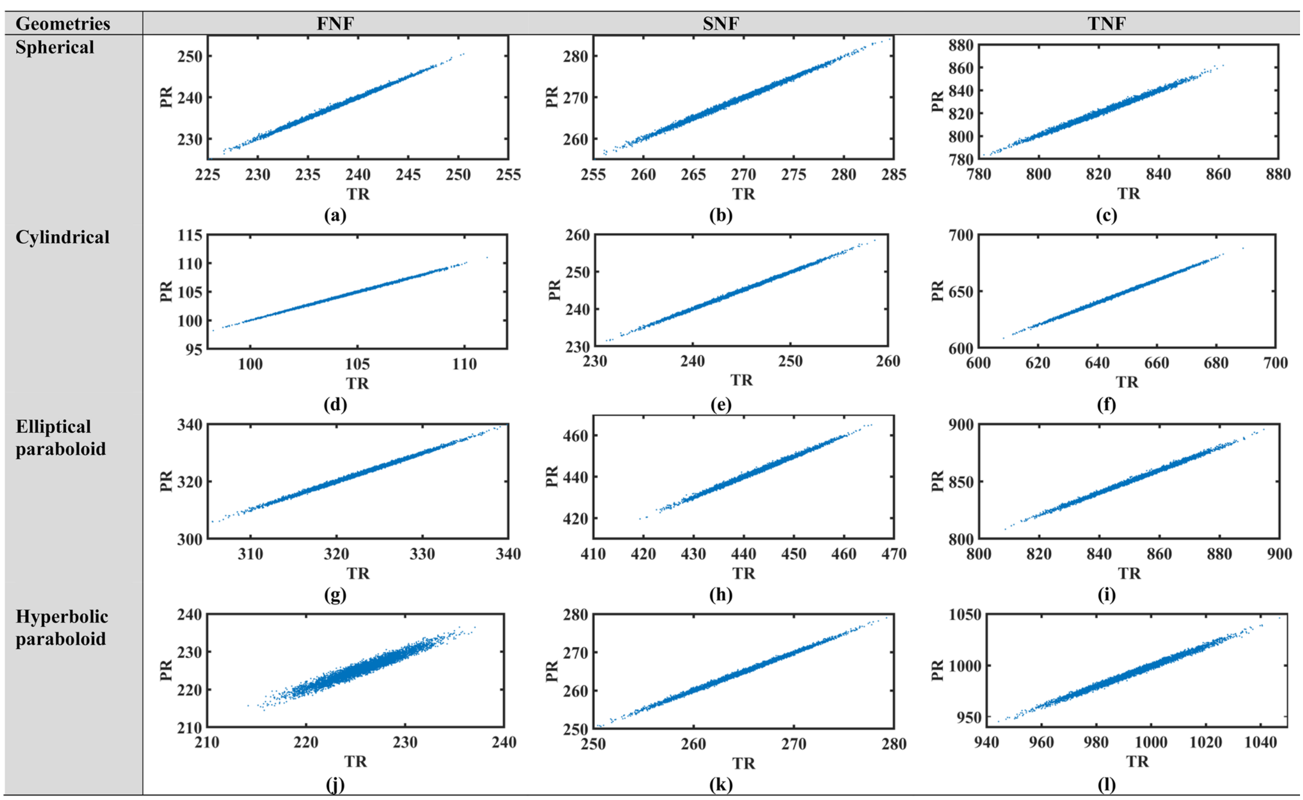

(d)

Fig. 7 (continued)

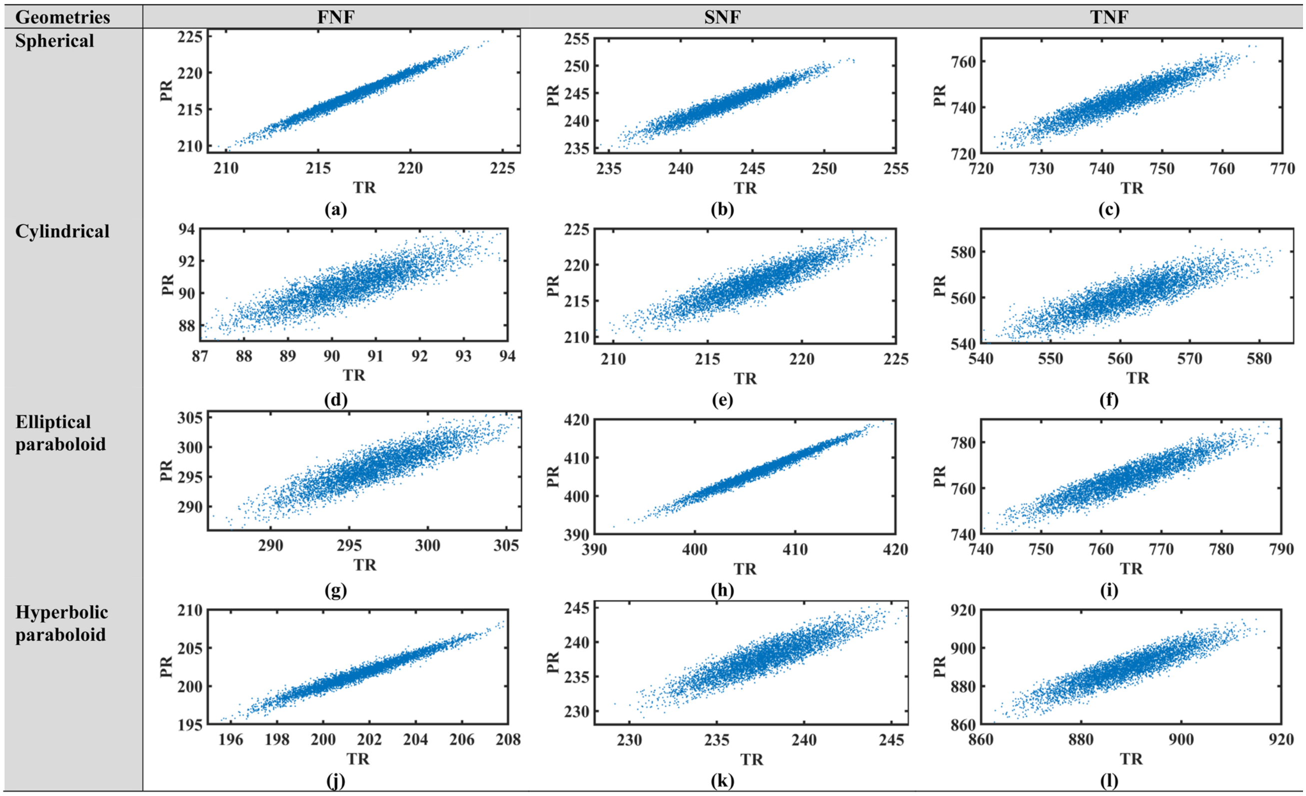

(e)

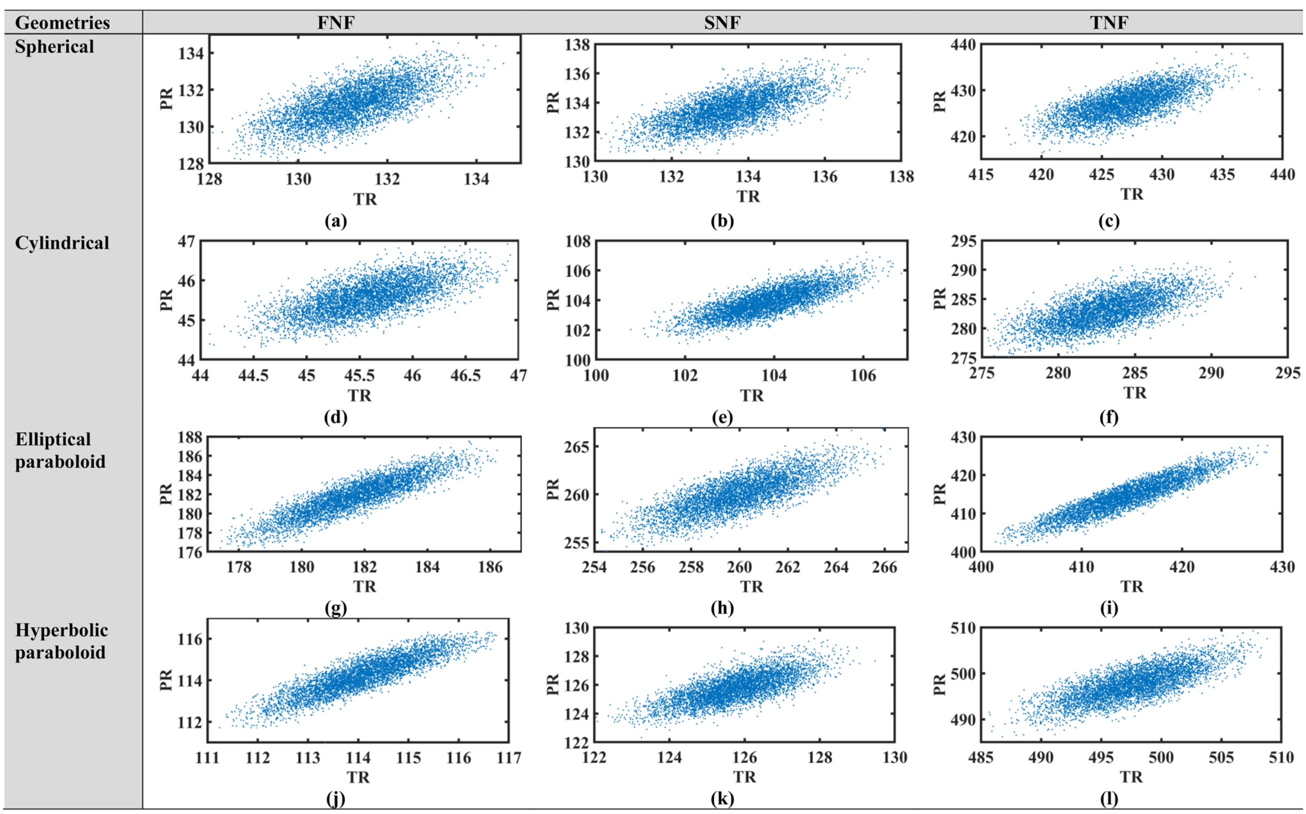

(f)

Fig. 7 (continued)

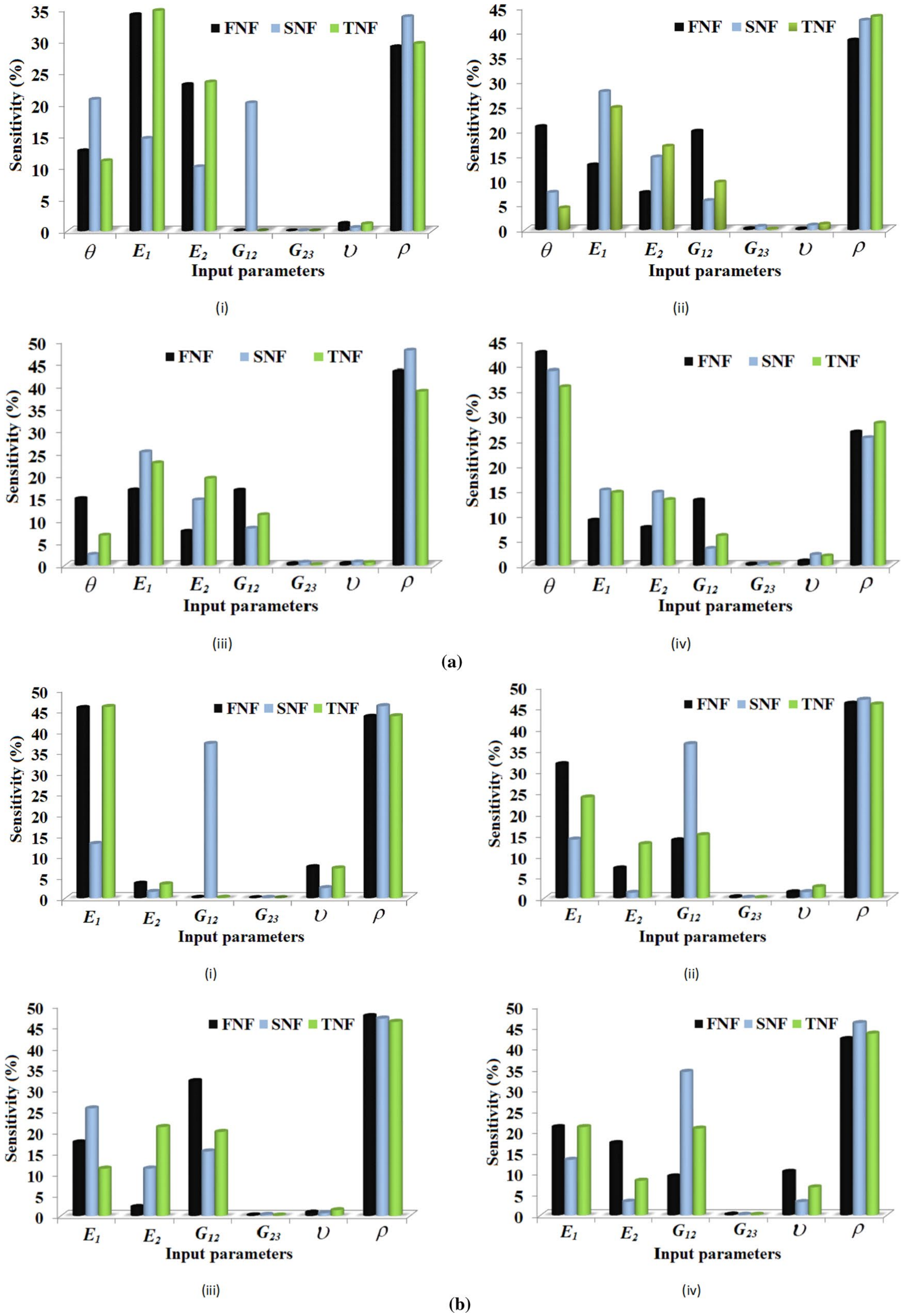

Fig. 8 Sensitivity analysis for the first three random natural frequencies (rad/s) for **a** case 1, **b** case 2, **c** case 3, **d** case 4, **e** case 5, and **f** case 6 considering various shell geometries (i) $S_{\mathrm{cyl.}}$, (ii) $S_{\mathrm{sph.}}$, (iii) $S_{\mathrm{ell.}}$ and (iv) $S_{\mathrm{hyp.}}$

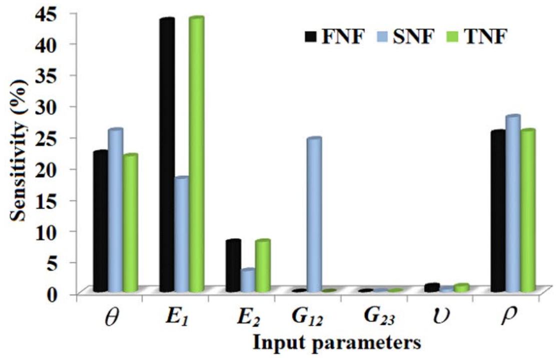

(i)

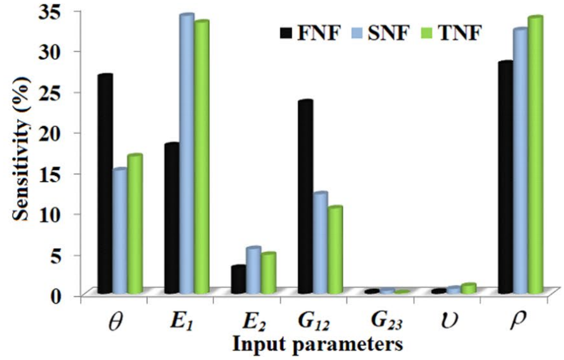

(ii)

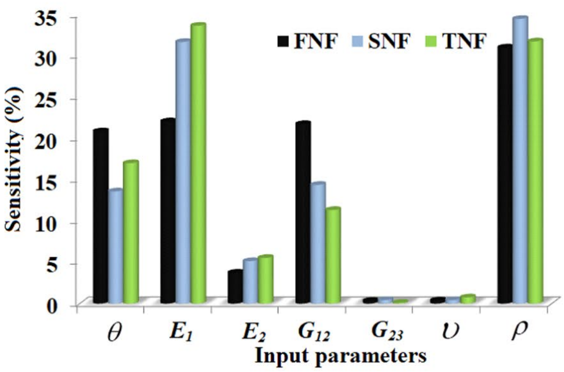

(iii)

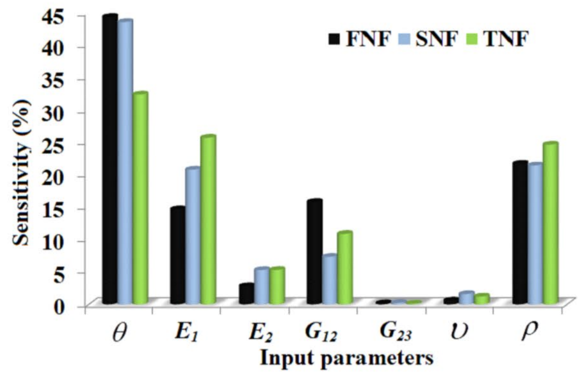

(iv)

(c)

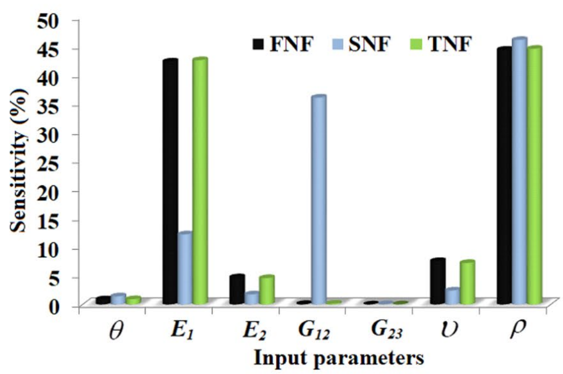

(i)

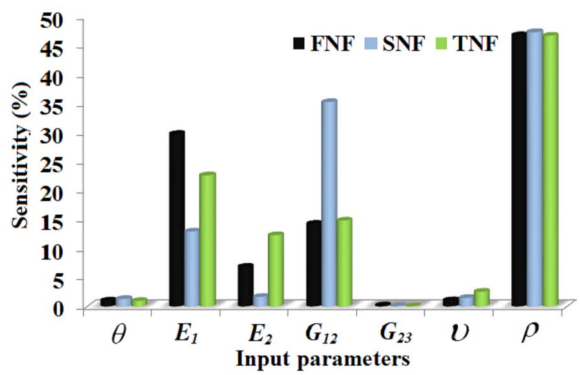

(ii)

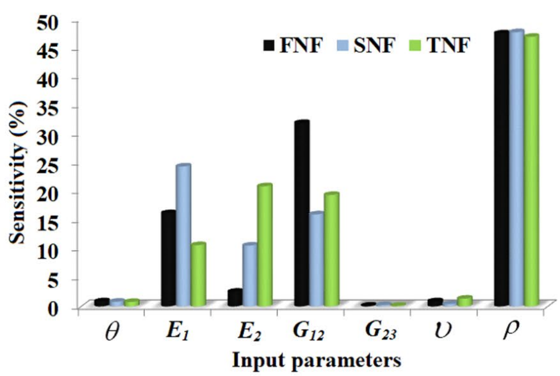

(iii)

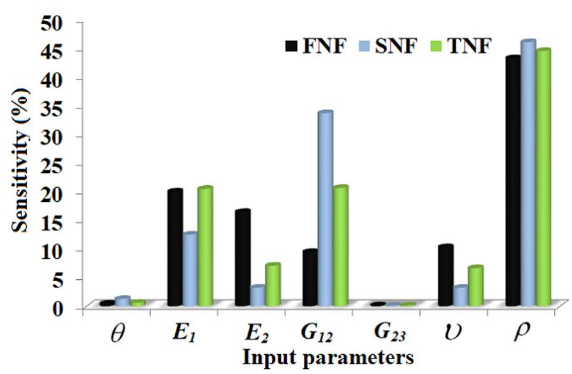

(iv)

(d)

Fig. 8 (continued)

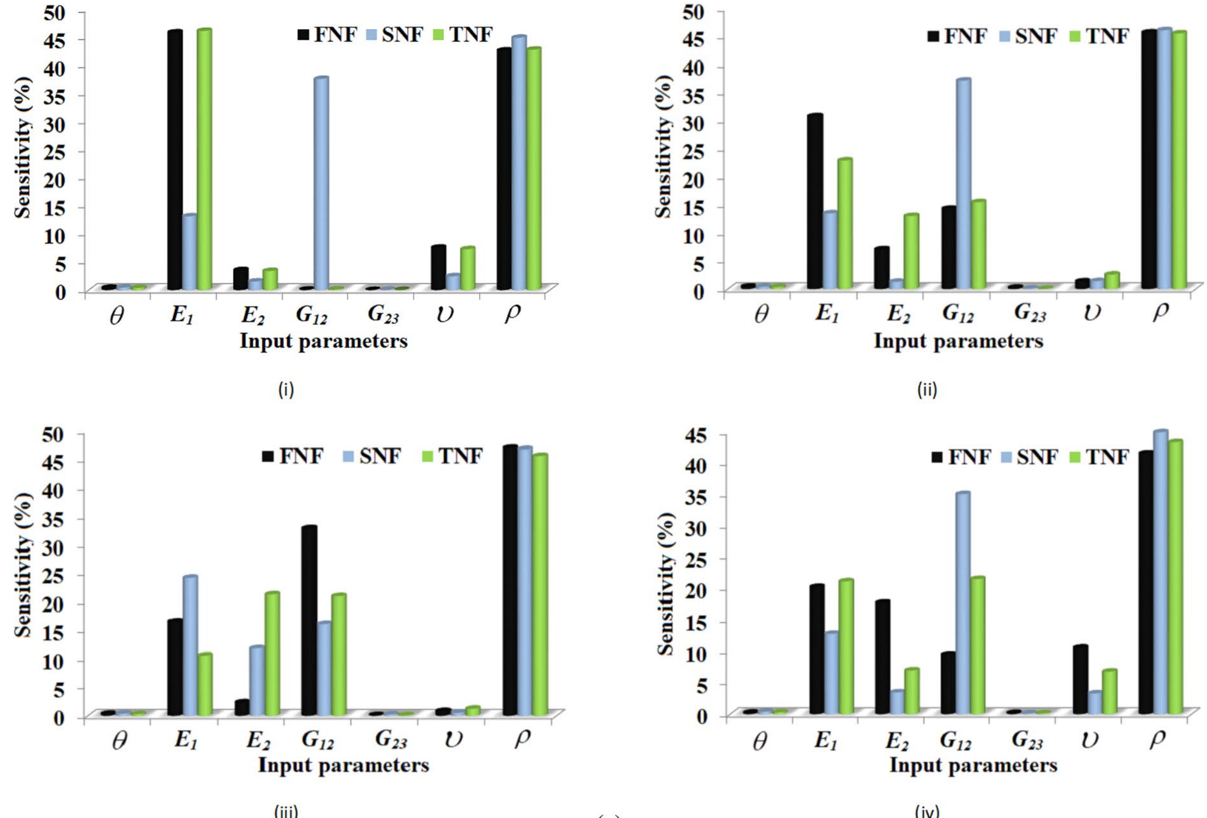

(e)

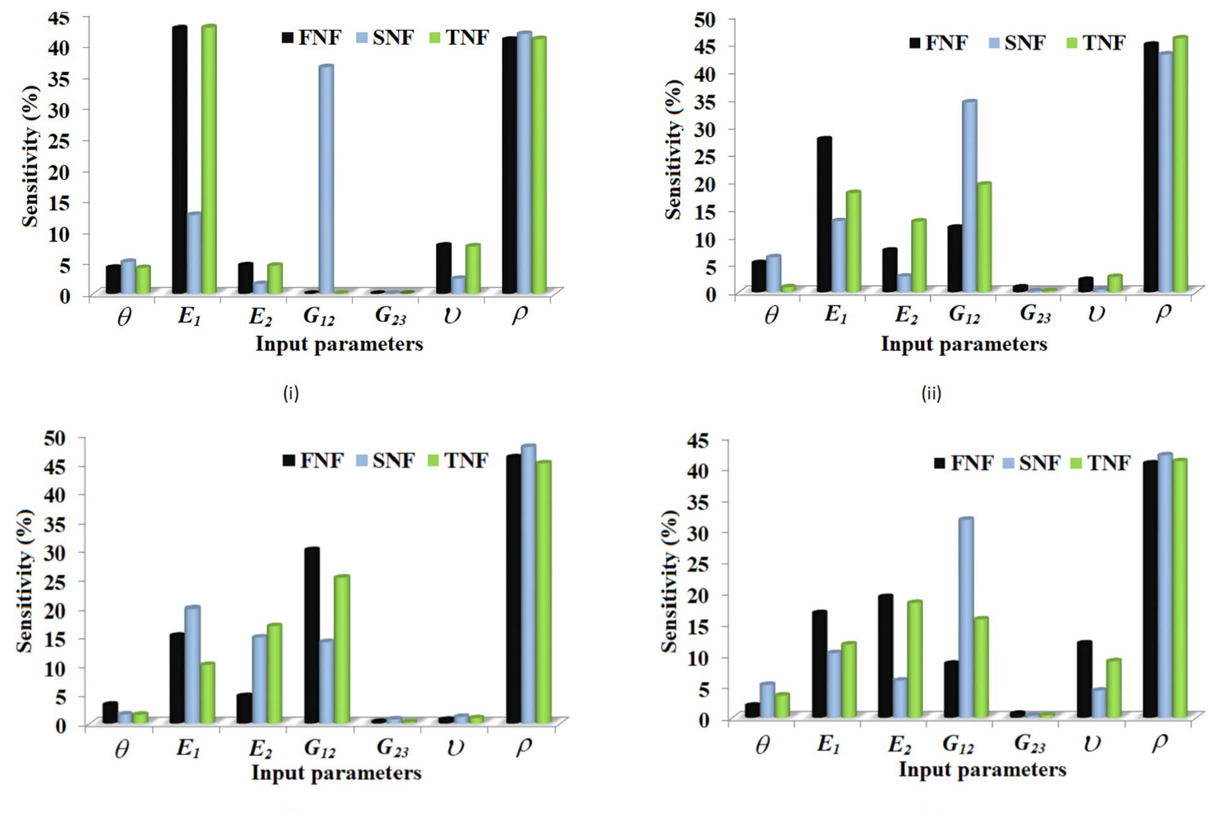

(f)

Fig. 8 (continued)

control. The present study focuses on the sensitivity of frequency responses of hybrid FG-sandwich structures with multi-functional applications. This study is helpful for establishing a unified measure in the case of multi-objective performances. In these hybrid structures, the advantages of each constituting component could potentially be exploited in a single structure. Such a construction could be helpful where the surface is exposed to extreme temperature or environmental conditions. However, an optimum lightweight design can still be achieved based on composite construction and depth-wise gradation towards the center of the shell. A novel MARS-based sensitivity analysis of these hybrid multi-functionally graded sandwich shells is developed to achieve computational efficiency without compromising with the outcome. Such surrogate-assisted FE approaches are crucial for computationally intensive multi-objective systems. It enumerates the degree of influence of various random input variables in the case of dynamic frequency responses. The MARS surrogate model is coupled with a finite element model to achieve computational efficacy (time and cost reduction). The numerical results indicate the proportional dominance of several random input parameters. Such analysis can provide the most significant parameters and their relative degree of importance in the multi-dimensional structural systems to design safe and reliable materials. It will lead to more optimized designs and better quality control while manufacturing the complex advanced structural systems. The results obtained showcase the sensitivity of the various input parameters like material properties and ply-orientation angle for first three natural frequencies. In most cases it is noted that mass density is the most sensitive parameter. Implementing different structural forms with different geometries in the present study will a vital role in the aerospace, civil construction, marine, naval, and automobile sectors. The detailed sensitivity analysis offers in-depth structure performance and characteristic understanding. The design paradigms can be enhanced, and a compelling performance can be obtained. Thus, the contribution of this article lies in both the development of a computationally efficient sensitivity analysis approach and the insightful numerical results for hybrid structures presented thereafter. The comprehensive and collective sensitivity quantification considering multi-functional objectives, as presented in this article, would lead to efficient computational modelling of complex structural systems for more optimized designs and better quality control during manufacturing. For further study, the computationally efficient uncertainty approach developed in this article can be utilised to investigate the effect of uncertainties in various other structures.

Acknowledgements The first author acknowledges the Ministry of Education (MoE), Government of India, for the financial support during this research work. The second author acknowledges the Aeronautics Research and Development Board (AR&DB), Government of India, for the financial support during this research work.

Author Contributions The first author acquired supervision, methodology, software and contributed to investigation and data curation, conceptualization, writing—original draft. SK acquired methodology, and provided resources and contributed to writing. SD, PKK and RRK provided resources and contributed to writing.

Data availability The data and materials in this paper are available.

Declarations

Conflict of interest The authors declare that they have no known conflicts of interest for the work reported in this paper.

References

1. Chandrashekhar M, Ganguli R (2010) Nonlinear vibration analysis of composite laminated and sandwich plates with random material properties. Int J Mech Sci 52(7):874–891
2. Pandit MK, Singh BN, Sheikh AH (2010) Vibration of sandwich plates with random material properties using improved higher-order zig-zag theory. Mech Adv Mater Struct 17(7):561–572
3. Arunkumar MP, Pitchaimani J, Gangadharan KV, Babu ML (2016) Influence of nature of core on vibro acoustic behavior of sandwich aerospace structures. Aerosp Sci Technol 56:155–167
4. Kavalur P, Jeyaraj P, Babu GR (2014) Static behaviour of visco-elastic sandwich plate with nano-composite facings under mechanical load. Procedia Materials Science 5:1376–1384
5. Tornabene F, Fantuzzi N, Bacciocchi M, Reddy JN (2017) An equivalent layer-wise approach for the free vibration analysis of thick and thin laminated and sandwich shells. Appl Sci 7(1):17
6. Farooq U, Ahmad MS, Rakha SA, Ali N, Khurram AA, Subhani T (2017) Interfacial mechanical performance of composite honeycomb sandwich panels for aerospace applications. Arab J Sci Eng 42(5):1775–1782
7. Van Tung H (2015) Thermal and thermo mechanical postbuckling of FGM sandwich plates resting on elastic foundations with tangential edge constraints and temperature-dependent properties. Compos Struct 131:1028–1039
8. Natarajan S, Manickam G (2012) Bending and vibration of functionally graded material sandwich plates using an accurate theory. Finite Elem Anal Des 57:32–42
9. Vaishali, Mukhopadhyay T, Kumar RR, Dey S (2020) Probing the multi-physical probabilistic dynamics of a novel functional class of hybrid composite shells. Compos Struct 262:113294
10. Zenkour AM (2005) A comprehensive analysis of functionally graded sandwich plates: part 1—deflection and stresses. Int J Solids Struct 42(18–19):5224–5242
11. Zenkour AM, Alghamdi NA (2008) Thermoelastic bending analysis of functionally graded sandwich plates. J Mater Sci 43(8):2574–2589
12. Das M, Barut A, Madenci E, Ambur DR (2006) A triangular plate element for thermo-elastic analysis of sandwich panels with a functionally graded core. Int J Numer Methods Eng 68(9):940–966

13. Li Q, Iu VP, Kou KP (2008) Three-dimensional vibration analysis of functionally graded material sandwich plates. J Sound Vib 311(1–2):498–515
14. Kashtalyan M, Menshykova M (2009) Three-dimensional elasticity solution for sandwich panels with a functionally graded core. Compos Struct 87(1):36–43
15. Vaishali M, T., Karsh, P.K., Basu, B. and Dey, S., (2020) Machine learning based stochastic dynamic analysis of functionally graded shells. Compos Struct 237:111870
16. Areias P, Rabczuk T, Msekh M (2016) Phase-field analysis of finite-strain plates and shells including element subdivision. Comput Methods Appl Mech Eng 312:322–350
17. Areias P, Rabczuk T (2013) Finite strain fracture of plates and shells with configurational forces and edge rotations. Int J Numer Meth Eng 94(12):1099–1122
18. Nguyen-Thanh N, Zhou K, Zhuang X, Areias P, Nguyen-Xuan H, Bazilevs Y, Rabczuk T (2017) Isogeometric analysis of large-deformation thin shells using RHT-splines for multiple-patch coupling. Comput Methods Appl Mech Eng 316:1157–1178
19. Fleck NA, Deshpande VS (2004) The resistance of clamped sandwich beams to shock loading. J Appl Mech 71(3):386–401
20. Cui X, Zhao L, Wang Z, Zhao H, Fang D (2012) A lattice deformation based model of metallic lattice sandwich plates subjected to impulsive loading. Int J Solids Struct 49(19–20):2854–2862
21. Zhu F, Wang Z, Lu G, Nurick G (2010) Some theoretical considerations on the dynamic response of sandwich structures under impulsive loading. Int J Impact Eng 37(6):625–637
22. Qin QH, Wang TJ (2009) An analytical solution for the large deflections of a slender sandwich beam with a metallic foam core under transverse loading by a flat punch. Compos Struct 88(4):509–518
23. Qin Q, Yuan C, Zhang J, Wang TJ (2014) Large deflection response of rectangular metal sandwich plates subjected to blast loading. Eur J Mech A Solids 47:14–22
24. Dharmasena KP, Wadley HN, Xue Z, Hutchinson JW (2008) Mechanical response of metallic honeycomb sandwich panel structures to high-intensity dynamic loading. Int J Impact Eng 35(9):1063–1074
25. Cui X, Zhao L, Wang Z, Zhao H, Fang D (2012) Dynamic response of metallic lattice sandwich structures to impulsive loading. Int J Impact Eng 43:1–5
26. Zhu F, Zhao L, Lu G, Wang Z (2008) Structural response and energy absorption of sandwich panels with an aluminium foam core under blast loading. Adv Struct Eng 11(5):525–536
27. Jamil A, Guan ZW, Cantwell WJ, Zhang XF, Langdon GS, Wang QY (2019) Blast response of aluminium/thermoplastic polyurethane sandwich panels–experimental work and numerical analysis. Int J Impact Eng 127:31–40
28. Reyes G (2010) Mechanical behavior of thermoplastic FML-reinforced sandwich panels using an aluminum foam core: experiments and modeling. J Sandwich Struct Mater 12(1):81–96
29. Kiratisaevee H, Cantwell WJ (2004) The impact response of aluminum foam sandwich structures based on a glass fiber-reinforced polypropylene fiber-metal laminate. Polym Compos 25(5):499–509
30. Liu C, Zhang YX, Li J (2017) Impact responses of sandwich panels with fibre metal laminate skins and aluminium foam core. Compos Struct 182:183–190
31. Liu C, Zhang YX, Ye L (2017) High velocity impact responses of sandwich panels with metal fibre laminate skins and aluminium foam core. Int J Impact Eng 100:139–153
32. Baştürk SB, Tanoğlu M, Çankaya MA, Eğilmez OÖ (2016) Dynamic behavior predictions of fiber-metal laminate/aluminum foam sandwiches under various explosive weights. J Sandwich Struct Mater 18(3):321–342
33. Tahir SI, Chikh A, Tounsi A, Al-Osta MA, Al-Dulaijan SU, Al-Zahrani MM (2021) Wave propagation analysis of a ceramic-metal functionally graded sandwich plate with different porosity distributions in a hygro-thermal environment. Compos Struct 269:114030
34. Avcar M, Hadji L, Civalek Ö (2021) Natural frequency analysis of sigmoid functionally graded sandwich beams in the framework of high order shear deformation theory. Compos Struct 276:114564
35. Kouider D, Kaci A, Selim MM, Bousahla AA, Bourada F, Tounsi A, Tounsi A, Hussain M (2021) An original four-variable quasi-3D shear deformation theory for the static and free vibration analysis of new type of sandwich plates with both FG face sheets and FGM hard core. Steel Compos Struct 41(2):167–191
36. Hadji L, Avcar M (2020) Free vibration analysis of FG porous sandwich plates under various boundary conditions. J Appl Comput Mechs. https://doi.org/10.22055/JACM.2020.35328.2628
37. Zaitoun MW, Chikh A, Tounsi A, Sharif A, Al-Osta MA, Al-Dulaijan SU, Al-Zahrani MM (2021) An efficient computational model for vibration behavior of a functionally graded sandwich plate in a hygrothermal environment with viscoelastic foundation effects. Eng Comput 1–15
38. Talebizad A, Isavand S, Bodaghi M, Shakeri M, Mohandesi JA (2013) Thermo-mechanical behavior of cylindrical pressure vessels made of functionally graded austenitic/ferritic steels. Int J Mech Sci 77:171–183
39. Zhao X, Liew KM (2011) Free vibration analysis of functionally graded conical shell panels by a meshless method. Compos Struct 93(2):649–664
40. Bodaghi M, Shakeri M (2012) An analytical approach for free vibration and transient response of functionally graded piezoelectric cylindrical panels subjected to impulsive loads. Compos Struct 94(5):1721–1735
41. Mudhaffar IM, Tounsi A, Chikh A, Al-Osta MA, Al-Zahrani MM, Al-Dulaijan SU (2021) Hygro-thermo-mechanical bending behavior of advanced functionally graded ceramic metal plate resting on a viscoelastic foundation. Structures, vol 33. Elsevier, Hoboken, pp 2177–2189
42. Hachemi H, Bousahla AA, Kaci A, Bourada F, Tounsi A, Benrahou KH, Tounsi A, Al-Zahrani MM, Mahmoud SR (2021) Bending analysis of functionally graded plates using a new refined quasi-3D shear deformation theory and the concept of the neutral surface position. Steel Compos Struct 39(1):51–64
43. Soldatos K, Aydogdu M, Gul U (2019) Plane strain polar elasticity of fibre-reinforced functionally graded materials and structures. J Mech Mater Struct 14(4):497–535
44. Zhu S, Ni Y, Sun J, Tong Z, Zhou Z, Xu X (2019) Accurate buckling analysis of piezoelectric functionally graded nanotube-reinforced cylindrical shells under combined electro-thermo-mechanical loads. J Mech Mater Struct 14(3):361–392
45. Zhang J, Zhang L, Li Y, Huang Y, Zhang H, Gao Y (2021) Free vibration of functionally graded piezoelectric hexagonal quasicrystal plates. J Mech Mater Struct 16(4):527–542
46. Hieu DV, Chan DQ, Sedighi HM (2021) Nonlinear bending, buckling and vibration of functionally graded nonlocal strain gradient nanobeams resting on an elastic foundation. J Mech Mater Struct 16(3):327–346
47. Zheng C, Mi C (2020) Analytical solutions for displacements and stresses in functionally graded thick-walled spheres subjected to a unidirectional outer tension. J Mech Mater Struct 15(5):585–603
48. Huang Y, Karami B, Shahsavari D, Tounsi A (2021) Static stability analysis of carbon nanotube reinforced polymeric composite doubly curved micro-shell panels. Arch Civ Mech Eng 21(4):1–15

49. Damanpack AR, Bodaghi MAHDI, Ghassemi HASSAN, Sayehbani MESBAH (2013) Boundary element method applied to the bending analysis of thin functionally graded plates. Latin Am J Solids Struct 10:549–570
50. Nayak P, Armani A (2021) Optimal three-dimensional design of functionally graded parts for additive manufacturing using Tamura–Tomota–Ozawa model. Proceedings of the Institution of Mechanical Engineers, Part L: Journal of Materials: Design and Applications 235(9):1993–2006
51. Moghaddam AM, Ahmadian MT, Kheradpisheh A (2013) Acoustic wave propagation through a functionally graded material plate with arbitrary material properties. Proceedings of the Institution of Mechanical Engineers, Part L: Journal of Materials: Design and Applications 227(2):100–110
52. Nikrad SF, Kanellopoulos A, Bodaghi M, Chen ZT, Pourasghar A (2021) Large deformation behavior of functionally graded porous curved beams in thermal environment. Arch Appl Mech 91(5):2255–2278
53. Sobhani E, Arbabian A, Civalek Ö, Avcar M (2021) The free vibration analysis of hybrid porous nanocomposite joined hemispherical–cylindrical–conical shells. Eng Comput. https://doi.org/10.1007/s00366-021-01453-0
54. Kumar RR, Mukhopadhyay T, Pandey KM, Dey S (2019) Stochastic buckling analysis of sandwich plates: the importance of higher order modes. Int J Mech Sci 152:630–643
55. Dey S, Mukhopadhyay T, Sahu SK, Adhikari S (2018) Stochastic dynamic stability analysis of composite curved panels subjected to non-uniform partial edge loading. Eur J Mech A Solids 67:108–122
56. Dey S, Mukhopadhyay T, Naskar S, Dey TK, Chalak HD, Adhikari S (2019) Probabilistic characterisation for dynamics and stability of laminated soft core sandwich plates. J Sandwich Struct Mater 21(1):366–397
57. Dey S, Mukhopadhyay T, Spickenheuer A, Adhikari S, Heinrich G (2016) Bottom up surrogate based approach for stochastic frequency response analysis of laminated composite plates. Compos Struct 140:712–727
58. Karsh PK, Mukhopadhyay T, Dey S (2018) Spatial vulnerability analysis for the first ply failure strength of composite laminates including effect of delamination. Compos Struct 184:554–567
59. Dey S, Mukhopadhyay T, Sahu SK, Adhikari S (2016) Effect of cutout on stochastic natural frequency of composite curved panels. Compos B Eng 105:188–202
60. Vaishali, Kumar RR, Dey S (2021) Dynamic sensitivity analysis of random impact behaviour of hybrid cylindrical shells. Recent advances in layered materials and structures. Springer, Singapore, pp 287–306
61. Kumar RR, Mukhopadhyay T, Naskar S, Pandey KM, Dey S (2019) Stochastic low-velocity impact analysis of sandwich plates including the effects of obliqueness and twist. Thin Walled Struct 145:106411
62. Ke S, Xu L, Ge Y (2018) Sensitivity analysis and estimation method of natural frequency for large cooling tower based on field measurement. Thin Walled Struct 127:809–821
63. Kotełko M, Lis P, Macdonald M (2017) Load capacity probabilistic sensitivity analysis of thin-walled beams. Thin Walled Struct 115:142–153
64. Deng L, Li J, Yang Y, Deng P (2020) Imperfection sensitivity analysis and DSM design of web-stiffened lipped channel columns experiencing local-distortional interaction. Thin Walled Struct 152:106699
65. Song X, Sun G, Li Q (2016) Sensitivity analysis and reliability based design optimisation for high-strength steel tailor welded thin-walled structures under crashworthiness. Thin Walled Struct 109:132–142
66. Kala Z (2011) Sensitivity analysis of stability problems of steel plane frames. Thin Walled Struct 49(5):645–651
67. Shahgholian-Ghahfarokhi D, Rahimi G (2020) A sensitivity study of the free vibration of composite sandwich cylindrical shells with grid cores. Iran J Sci Technol Trans Mech Eng 44(1):149–162
68. Ghazani MS, Binesh B, Fardi-Ilkhchy A (2019) Effect of strain rate sensitivity and strain hardening exponent of materials on plastic strain distribution and damage accumulation during equal channel angular pressing. Iran J Sci Technol Trans Mech Eng 43(1):831–844
69. Bernard SS, Jayakumari LS (2018) Pressure and temperature sensitivity analysis of palm fiber as a biobased reinforcement material in brake pad. J Braz Soc Mech Sci Eng 40(3):152
70. Di Sciuva M, Gherlone M, Lomario D (2003) Multiconstrained optimisation of laminated and sandwich plates using evolutionary algorithms and higher-order plate theories. Compos Struct 59(1):149–154
71. Rathbun HJ, Zok FW, Evans AG (2005) Strength optimisation of metallic sandwich panels subject to bending. Int J Solids Struct 42(26):6643–6661
72. Tan XH, Soh AK (2007) Multi-objective optimisation of the sandwich panels with prismatic cores using genetic algorithms. Int J Solids Struct 44(17):5466–5480
73. Icardi U, Ferrero L (2009) Optimisation of sandwich panels with functionally graded core and faces. Compos Sci Technol 69(5):575–585
74. Brockman RA, Lung FY (1988) Sensitivity analysis with plate and shell finite elements. Int J Numer Methods Eng 26(5):1129–1143
75. Lee KW, Park GJ (1997) Accuracy test of sensitivity analysis in the semi-analytic method with respect to configureuration variables. Comput Struct 63(6):1139–1148
76. Hamdia KM, Ghasemi H, Zhuang X, Alajlan N, Rabczuk T (2018) Sensitivity and uncertainty analysis for flexoelectric nanostructures. Comput Methods Appl Mech Eng 337:95–109
77. António CC, Hoffbauer LN (2013) Uncertainty assessment approach for composite structures based on global sensitivity indices. Compos Struct 99:202–212
78. Zhang Z, Zhan C, Shankar K, Morozov EV, Singh HK, Ray T (2017) Sensitivity analysis of inverse algorithms for damage detection in composites. Compos Struct 176:844–859
79. de Sousa BS, Gomes GF, Jorge AB, da Cunha Jr SS, AncelottiJr AC (2018) A modified topological sensitivity analysis extended to the design of composite multidirectional laminates structures. Compos Struct 200:729–746
80. Bishay PL, Sofi AR (2018) Sensitivity analysis of a smart soft composite robotic finger design using geometrically nonlinear laminated composite finite beam elements. Mater Today Commun 16:111–118
81. Zadeh FK, Nossent J, Sarrazin F, Pianosi F, van Griensven A, Wagener T, Bauwens W (2017) Comparison of variance-based and moment-independent global sensitivity analysis approaches by application to the SWAT model. Environ Model Softw 91:210–222
82. Zhao W, Bu L (2019) Global sensitivity analysis with a hierarchical sparse metamodeling method. Mech Syst Signal Process 115:769–781
83. Vu-Bac N, Lahmer T, Zhuang X, Nguyen-Thoi T, Rabczuk T (2016) A software framework for probabilistic sensitivity analysis for computationally expensive models. Adv Eng Softw 100:19–31
84. Zhao X, Lee YY, Liew KM (2009) Free vibration analysis of functionally graded plates using the element-free kp-Ritz method. J Sound Vib 319(3–5):918–939

85. Loy CT, Lam KY, Reddy JN (1999) Vibration of functionally graded cylindrical shells. Int J Mech Sci 41(3):309–324
86. Touloukian YS (1967) Thermophysical properties of high temperature solid materials: elements, vol 1. Macmillan, London
87. Dey S, Mukhopadhyay T, Spickenheuer A, Gohs U, Adhikari S (2016) Uncertainty quantification in natural frequency of composite plates—an artificial neural network based approach. Adv Compos Lett 25(2):096369351602500203
88. Saltelli A, Ratto M, Andres T, Campolongo F, Cariboni J, Gatelli D, Saisana M, Tarantola S (2008) Global sensitivity analysis: the primer. Wiley, Hoboken
89. Sobol IM (2001) Global sensitivity indices for nonlinear mathematical models and their Monte Carlo estimates. Math Comput Simul 55(1–3):271–280
90. Iman RL, Hora SC (1990) A robust measure of uncertainty importance for use in fault tree system analysis. Risk Anal 10(3):401–406
91. Homma T, Saltelli A (1996) Importance measures in global sensitivity analysis of nonlinear models. Reliab Eng Syst Saf 52(1):1–17
92. Mukhopadhyay T, Chakraborty S, Dey S, Adhikari S, Chowdhury R (2017) A critical assessment of Kriging model variants for high-fidelity uncertainty quantification in dynamics of composite shells. Arch Comput Methods Eng 24(3):495–518
93. Vaishali, Dey S (2021) Temperature-dependent random frequency of functionally graded spherical shells—a PCE approach. Recent advances in mechanical engineering. Springer, Singapore, pp 509–516
94. Gupta KK, Mukhopadhyay T, Roy A, Roy L, Dey S (2021) Sparse machine learning assisted deep computational insights on the mechanical properties of graphene with intrinsic defects and doping. J Phys Chem Solids 155:110111
95. Dey S, Mukhopadhyay T, Adhikari S (2017) Metamodel based high-fidelity stochastic analysis of composite laminates: a concise review with critical comparative assessment. Compos Struct 171:227–250
96. Mukhopadhyay T, Naskar S, Dey S, Adhikari S (2016) On quantifying the effect of noise in surrogate based stochastic free vibration analysis of laminated composite shallow shells. Compos Struct 140:798–805
97. Dey S, Mukhopadhyay T, Khodaparast HH, Adhikari S (2016) A response surface modelling approach for resonance driven reliability based optimisation of composite shells. Period Polytech Civ Eng 60(1):103–111
98. Gupta KK, Mukhopadhyay T, Roy L, Dey S (2021) Hybrid machine learning assisted quantification of the compound internal and external uncertainties of graphene: Towards inclusive analysis and design. Materials Advances. 3:1160–1181
99. Saha S, Gupta KK, Maity SR, Dey S (2021) Data-driven probabilistic performance of Wire EDM: A machine learning based approach. Proc Inst Mech Eng Part B J Eng Manuf 236:908–919
100. Kumar RR, Vaishali, Pandey KM, Dey S (2020) Effect of skewness on random frequency responses of sandwich plates. Recent advances in theoretical, applied, computational and experimental mechanics. Springer, Singapore, pp 13–20
101. Vaishali, Dey S (2021) Support vector model based thermal uncertainty on stochastic natural frequency of functionally graded cylindrical shells. Recent advances in computational mechanics and simulations. Springer, Singapore, pp 651–658
102. Friedman JH (1991) Multivariate adaptive regression splines. Ann Stat. https://doi.org/10.1214/aos/1176347963
103. Hastie T, Tibshirani R, Friedman J (2009) The elements of statistical learning: data mining, inference, and prediction. Springer, New York
104. Karsh PK, Mukhopadhyay T, Chakraborty S, Naskar S, Dey S (2019) A hybrid stochastic sensitivity analysis for low-frequency vibration and low-velocity impact of functionally graded plates. Compos B Eng 176:107221
105. Karsh PK, Thakkar B, Kumar RR, Dey S (2021) Probabilistic oblique impact analysis of functionally graded plates–a multivariate adaptive regression splines approach. Eur J Comput Mech. https://doi.org/10.13052/ejcm2642-2085.30234
106. Sobol IYM (1967) On the distribution of points in a cube and the approximate evaluation of integrals. Zhurnal Vychislitel'noi Matematikii Matematicheskoi Fiziki 7(4):784–802
107. Craven P, Wahba G (1978) Smoothing noisy data with spline functions. Numer Math 31(4):377–403
108. Singh H, Hazarika BC, Dey S (2017) Low velocity impact responses of functionally graded plates. Procedia Eng 173:264–270
109. Rizov V, Shipsha A, Zenkert D (2005) Indentation study of foam core sandwich composite panels. Compos Struct 69(1):95–102
110. Baferani AH, Saidi AR, Ehteshami H (2011) Accurate solution for free vibration analysis of functionally graded thick rectangular plates resting on elastic foundation. Compos Struct 93(7):1842–1853
111. Ta HD, Noh HC (2015) Analytical solution for the dynamic response of functionally graded rectangular plates resting on elastic foundation using a refined plate theory. Appl Math Model 39:6243–6257
112. Sayyad AS, Ghugal YM (2021) Static and free vibration analysis of doubly-curved functionally graded material shells. Compos Struct 269:114045
113. Hull R, Keblinski P, Lewis D, Maniatty A, Meunier V, Oberai AA, Picu CR, Samuel J, Shephard MS, Tomozawa M, Vashishth D (2018) Stochasticity in materials structure, properties, and processing—a review. Appl Phys Rev 5(1):011302